Cyclopropane-Derived Peptidomimetics. Design, Synthesis, Evaluation, and Structure of Novel HIV-1 Protease Inhibitors

Stephen F. Martin,* Gordon O. Dorsey, Todd Gane, and Michael C. Hillier

Department of Chemistry and Biochemistry, The University of Texas, Austin, Texas 78712

Horst Kessler,* Matthias Baur, and Barbara Mathä

Institut für Organische Chemie und Biochemie, Technische Universität München, D-85747 Garching, Germany

John W. Erickson,* T. Nagarajan Bhat, Sanjeev Munshi, Sergei V. Gulnik, and Igor A. Topol

Structural Biochemistry Program, Frederick Biomedical Supercomputing Center, NCI-FCRDC, Frederick, Maryland 21702

Received January 15, 1998

Toward establishing the general efficacy of using trisubstituted cyclopropanes as peptide mimics to stabilize extended peptide structures, the cyclopropanes **20a**−**d** were incorporated as replacements into **9**−**13**, which are analogues of the known HIV-1 protease inhibitors **14** and **15**. The syntheses of **20a**−**d** commenced with the Rh_2[5(*S*)-MEPY]$_4$-catalyzed cyclization of the allylic diazoesters **16a**−**d** to give the cyclopropyl lactones **17a**−**d** in high enantiomeric excess. Opening of the lactone moiety using the Weinreb protocol and straightforward refunctionalization of the intermediate amides **18a**−**d** gave **20a**−**d**. A similar sequence of reactions was used to prepare the *N*-methyl-2-pyridyl analogue **28**. Coupling of **20a**−**d** and **28** with the known diamino diol **22** delivered **9**−**13**. Pseudopeptides **9**−**12** were found to be competitive inhibitors of wild-type HIV-1 protease in biological assays having K_is of 0.31−0.35 nM for **9**, 0.16−0.21 nM for **10**, 0.47 nM for **11**, and 0.17 nM for **12**; these inhibitors were thus approximately equipotent to the known inhibitor **14** (IC_{50} = 0.22 nM) from which they were derived. On the other hand **13** (K_i = 80 nM) was a weaker inhibitor than its analogue **15** (K_i = 0.11 nM). The solution structures of **9** and **10** were analyzed by NMR spectroscopy and simulated annealing procedures that included restraints derived from homo- and heteronuclear coupling constants and NOEs; because of the molecular symmetry of **9** and **10,** a special protocol to treat the NOE data was used. The final structure was checked by restrained and free molecular dynamic calculations using an explicit DMSO solvent box. The preferred solution conformations of **9** and **10** are extended structures that closely resemble the three-dimensional structure of **10** bound to HIV-1 protease as determined by X-ray crystallographic analysis of the complex. This work convincingly demonstrates that extended structures of peptides may be stabilized by the presence of substituted cyclopropanes that serve as peptide replacements. Moreover, the linear structure enforced in solution by the two cyclopropane rings in the pseudopeptides **9**−**12** appears to correspond closely to the biologically active conformation of the more flexible inhibitors **14** and **15**. The present work, which is a combination of medicinal, structural, and quantum chemistry, thus clearly establishes that cyclopropanes may be used as structural constraints to reduce the flexibility of linear pseudopeptides and to help enforce the biologically active conformation of such ligands in solution.

Introduction

One of the exciting challenges in contemporary bioorganic chemistry is determining the three-dimensional structural details of the complexes of biologically active oligopeptides and their derivatives with enzyme active sites or receptors. Such studies provide critical information that may be exploited to design new ligands with even higher binding affinities for the macromolecular binding site. When a direct investigation of the complex is not possible, one common approach to gain insights into the topological requirements within the host−guest complex involves the elucidation of the biologically active conformation of the peptide ligand. However, linear oligopeptides interconvert rapidly in solution between a number of conformations differing little in energy, and the knowledge of the preferred solution conformation(s) of an oligopeptide does not necessarily provide information regarding the conformation of that ligand when bound to its respective host.[1] In the absence of three-dimensional structural data for the ligand−receptor complex itself, information relating to the biologically active conformation of oligopeptide ligands has been generally obtained by introducing conformational restraints by cyclization or by incorporation of peptide mimics at selected sites on the peptide backbone.[2−5] The resultant effects upon binding and biological activity of the resulting pseudopeptides are then evaluated in connection with available reduced conformational space to provide insights into the biologically active conformation of the ligand.

S0022-2623(98)00033-8 CCC: $15.00
Published on Web 04/17/1998

Scheme 1

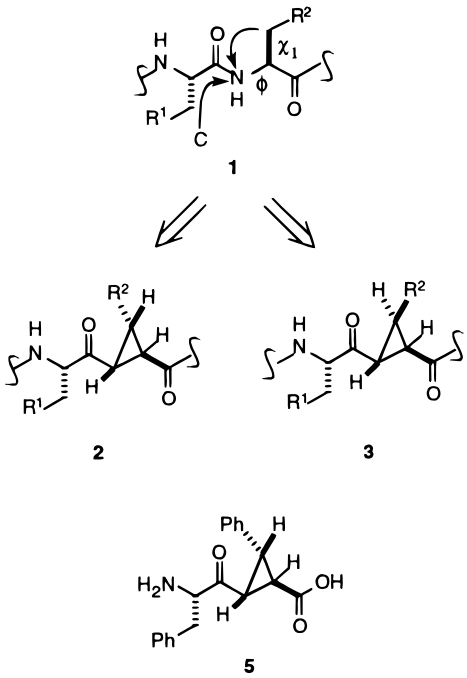

Most of the conformationally restricted replacements of peptide secondary structure reported to date imitate turns, or helices. Inasmuch as peptide substrates generally appear to bind to proteases in extended conformations, the design of structural elements mimicking β-strand arrays is an important, albeit more difficult, challenge. Recently there have been several reports of peptide mimics that enforce extended structure although they make no provision for orienting the side chains.[6] The importance of controlling the side chain orientations of pseudopeptides has been recognized because these appendages provide crucial sites for recognition, specificity, binding, and consequent transduction.[7] Consequently, we initiated a research program to design and develop dipeptide replacements that would enforce an extended (β-strand) conformation on the backbone of oligopeptides while projecting the amino acid side chains in specific orientations.

Design. On the basis of a series of molecular modeling studies, we postulated that the 1,2,3-trisubstituted cyclopropanes **2** and **3**, which shall be generally denoted as −XaaΨ[COcpCO]Yaa−, would constitute novel rigid, isosteric replacements of an extended conformation of the dipeptide moiety **1** (Scheme 1). Operationally, **2** and **3**, which differ from the more common 1-aminocyclopropanecarboxylic acids,[8] are derived from **1** by replacing the amide nitrogen with a carbon and forming a single bond between this atom and C(β) on the amino acid side chain.[9] The peptide backbone in both **2** and **3** is locally rigidified in a β-strand conformation by locking the ϕ angle at about −120°. Another factor that contributes to the overall rigidity induced by this surrogate is the preferred conformation, which is a consequence of steric and electronic effects, about the carbon−carbon bond between the carbonyl group and the cyclopropane.[10]

The portion of the amino acid side chain designated as R^2 in the cyclopropane-derived dipeptide surrogate **2** occupies approximately the same region of space *relative to the backbone* that it would if the corresponding amino acid residue in **1** were locked in the gauche(−) conformation in which the χ_1-angle is about −60°. The geometric properties of replacements of type **2** may be better illustrated by examining the superimposition of the −PheΨ[COcpCO]Phe− replacement **5**, in which the N-terminal Phe is also anchored in the gauche(−) conformation, with the corresponding Phe-Phe dipeptide in which the backbone is in an idealized β-strand and both phenyl groups are fixed in gauche(−) orientations (Figure 1). The root-mean-square (rms) fit for this rigid superimposition is approximately 0.35 Å. In a similar fashion, the spatial orientation of the R^2 group in the epimeric replacement **3** mimics that found when the side chain of the C-terminal residue in **1** is constrained in the gauche(+) conformation wherein the χ_1-angle is about +60°.

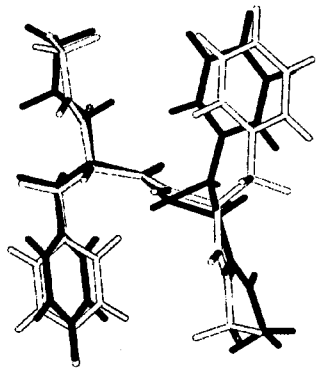

Figure 1. A rigid superimposition of −PheΨ[COcpCO]Phe− surrogate **5** with a Phe-Phe dipeptide in which the backbone is in an idealized β-strand and the two phenyl groups are fixed in gauche(−) orientations.

Although some hydrogen-bonding capability of an amide carbonyl group is maintained by the keto functions in the rigid isosteres **2** and **3**, deletion of a backbone N−H in these surrogates eliminates one possible intermolecular hydrogen bond to a receptor or enzyme. However, the actual importance of losing this hydrogen bond is difficult to assess a priori since other peptide replacements that lack hydrogen-bonding ability (e.g., double bonds) are known to be efficacious in certain cases. The entropic advantage that arises from restricting the rotors (0.8−1.2 kcal/rotor) associated with the ϕ- and the χ_1-angles in the constrained pseudopeptide could approximately compensate the energetic cost of losing one intermolecular hydrogen bond, (0.5−1.8 kcal/H-bond) *provided the receptor bound conformation is well-matched*.[11,12] It must also be recognized that consequent to the mutation of the dipeptide **1** into **2** or **3** amide resonance and the associated hindered rotation about the amide −C(=O)N bond is lost, so there is not a *net* restriction of two full rotors.

Preliminary modeling studies suggested that trisubstituted cyclopropanes related to **2** and **3** would serve as rigid mimics of localized β-strand structure. To evaluate this hypothesis we first incorporated N-terminal truncated analogues of **2** and **3** at the P3 position of conformationally restricted analogues of the aspartic proteinase renin.[13] We discovered that **6**, which bears an N-terminal amide group rather than the keto function of the parent **2**, was a subnanomolar inhibitor of renin.[13a] Since **6** was approximately equipotent with

the corresponding flexible analogue **7**, it seems probable that the two inhibitors bind to the active site of renin in closely similar conformations and that the cyclopropane ring in **6** orients the aromatic side chain at the P3 subsite in the biologically active conformation of **7**. We then began to exploit cyclopropane-containing inhibitors as topographical probes of the bound conformation of collagenase inhibitors and other biologically active pseudopeptides.[14] Others have recently incorporated replacements related to **2** and **3** in non-peptide fibrinogen receptor antagonists.[15]

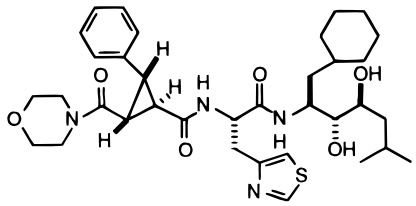

6

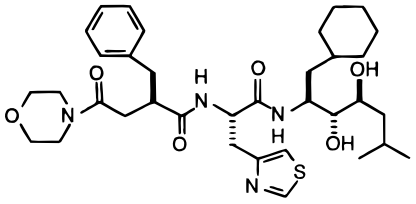

7

While these early investigations began to establish the efficacy of trisubstituted cyclopropanes as novel peptide mimics, a number of important questions remain. For example, can more than one cyclopropane replacement be incorporated into a flexible enzyme inhibitor to further rigidify the structure and stabilize the biologically active conformation? Can the cyclopropane subunit(s) be positioned closer to the site of the "scissile amide bond" (i.e., the P1−P1′ juncture) without loss of potency? To address these critical issues, we queried whether cyclopropane-derived peptide isosteres might be introduced into conformationally constrained inhibitors of HIV-1 protease, an aspartic proteinase that is responsible for the release of protease, reverse transcriptase, and integrase from the *gag-pol* fusion protein of the HIV-1 virus.[16,17] Numerous X-ray structures of HIV-1 protease complexed with inhibitors reveal that the inhibitors typically bind to the enzyme active site clefts in an extended β-strand conformation in which the three-dimensional structure of the bound inhibitors is very similar for the P2−P2′ segment of the backbone. It thus occurred to us that a biological and structural study of the pseudopeptides **9**−**13**, which are derivatives of the known inhibitors **14** (A-75925, $IC_{50} = 0.22$ nM)[16d] and **15** (A-76889, $K_i = 0.11$ nM),[17d] would elicit some additional insights regarding the scope and limitations of −XaaΨ[COcpCO]Yaa− replacements. Each of the pseudopeptides **9**−**13** contain *two* N-terminal truncated −XaaΨ[COcpCO]Yaa− replacements, *and* these replacements are incorporated one residue closer (i.e., the P2 and P2′ subsites) to the scissile bond than in the renin inhibitor **6** (i.e., the P3 subsite). We now report the syntheses and biological evaluation of the pseudopeptides **9**−**13** together with a comparison of the solution structures of **9** and **10**, which were determined using NMR techniques and molecular dynamics (MD) calculations, with the biologically active conformation of **10**, which was determined by X-ray analysis of the complex of **10** bound to the active site of HIV-1 protease.

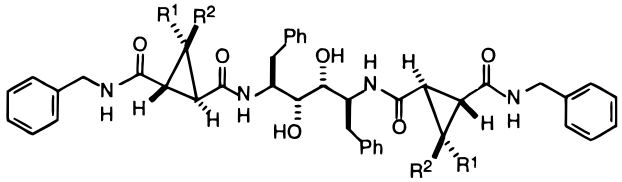

9: $R^1 = R^2 = Me$
10: $R^1 = Me$; $R^2 = H$
11: $R^1 = H$; $R^2 = Me$
12: $R^1 = R^2 = H$

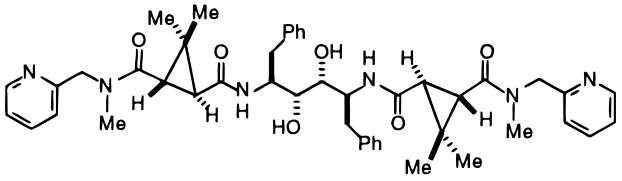

13

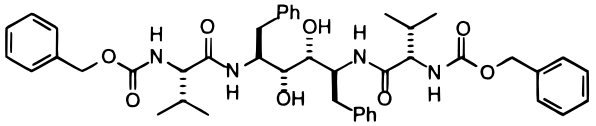

14

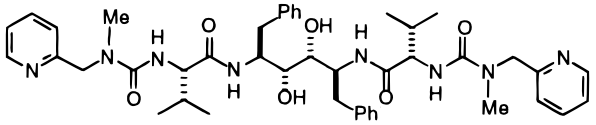

15

Results

Synthesis of Inhibitors. We envisioned that **9**−**12** could be prepared by coupling the enantiomerically pure carboxylic acids **20a**−**d** with the known diamino diol **22** (Scheme 2).[18] On the basis of prior experience, the simplest approach to these acids would involve application of our general procedures for asymmetric intramolecular cyclopropanations.[19] In the event, the allylic diazoacetates **16a**−**d**, which were prepared from the corresponding alcohols,[20] were heated in the presence of the chiral rhodium catalyst Rh_2[5(*S*)-MEPY]$_4$ to give the cyclopropyl lactones **17a**−**d** in 84−92% yield and 87−98% enantioselectivity. Subsequent opening of the lactone rings of **17a**−**d** with *N*-benzyl-*N*-(*p*-methoxyphenylmethyl)amine (MPMNHBn) was accomplished in 73−79% yield using the Weinreb protocol to give the amides **18a**−**d**, respectively.[21] Oxidation of the primary alcohol function in **18a**−**d** with pyridinium chlorochromate (PCC) gave the corresponding aldehydes (77−93%), which were epimerized to deliver **19a**−**d**. Jones oxidation of **19a**−**d** followed by removal of the methoxyphenylmethyl (MPM) protecting group with trifluoroacetic acid (TFA) furnished the requisite carboxylic acids **20a**−**d** in 60−69% yield. Reaction of **20a**−**d** with the diamino diol **22** under standard peptide coupling conditions using *N*-ethyl-*N*-(dimethylaminopropyl)carbodi-

Scheme 2

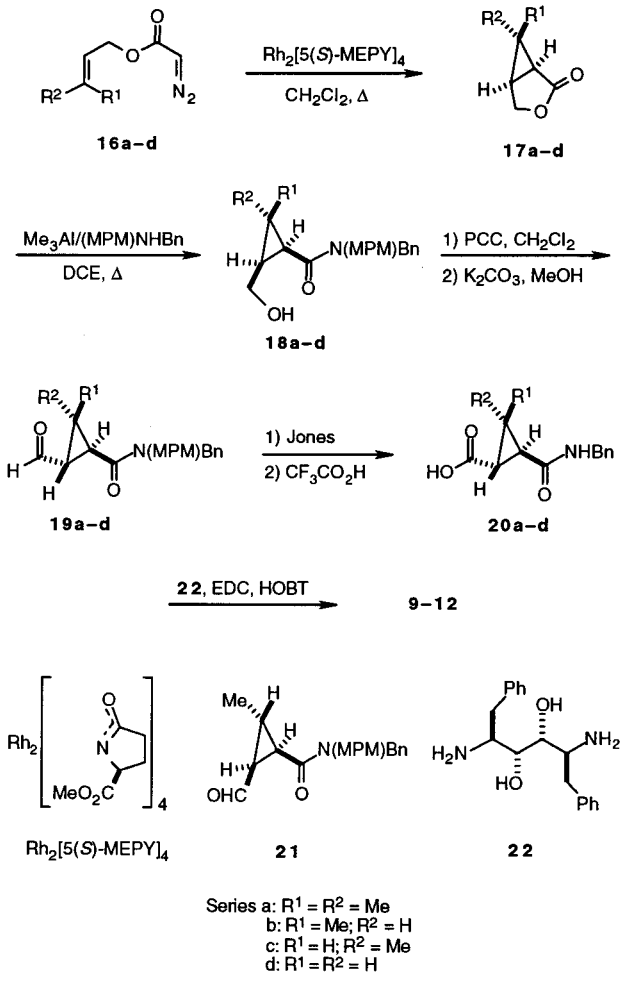

8

imide hydrochloride (EDC) and 1-hydroxybenzotriazole (HOBT) afforded the pseudopeptides **9**−**12** in 77−98% yield.

Although the epimerization of the aldehydes obtained by oxidation of **18a,b,d** proceeded to completion, only partial epimerization of **21** occurred, and an equilibrium mixture (40:60) of **21** and the desired aldehyde **19c** was obtained.[22] To address this inefficiency an alternate route to **20c** was developed (Scheme 3). In the event, the allylic diazo ester **16b** was cyclized in 78% yield and 92% ee upon heating in the presence of the enantiomeric dirhodium catalyst Rh_2[5(*R*)-MEPY]$_4$ to give **23**. Opening of the lactone ring with *N*-benzyl-*N*-(*p*-methoxyphenylmethyl)amine under Weinreb conditions gave **24**, which was subjected to the standard sequence of oxidation, epimerization, and deprotection to give **20c** in 60% overall yield from **23**.

The *N*-methyl-2-pyridyl analogue **13** was prepared by a sequence of reactions analogous to those presented in Scheme 4. Thus, amidation of the lactone **17a** with 2-aminomethyl pyridine in the presence of a catalytic amount of NaCN in methanol gave **25** in 98% yield. Protection of the primary alcohol as the *tert*-butyldimethylsilyl (TBDMS) ether, followed by methylation of the amide nitrogen using NaH and MeI and removal of the hydroxyl protecting group by the action of tetra-*n*-butylammonium fluoride (TBAF) afforded the *N*-methyl

Scheme 3

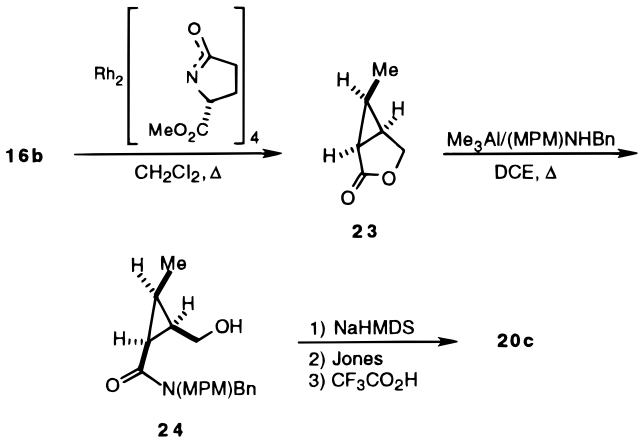

alcohol **26** in 74% overall yield. Oxidation of the primary alcohol with the Dess−Martin periodinane followed by epimerization of the resulting aldehyde afforded **27** in 78% overall yield. Oxidation of **27** with Jones reagent gave the acid **28** (55%), which was then coupled to the diamino diol **21** as previously described to furnish **14**.

Biological Activity. Compounds **9**−**12**, which are analogues of the known inhibitor **14**, were each found to be fast-binding, competitive inhibitors of wild-type HIV-1 protease; there was no evidence for slow binding. The potencies of these pseudopeptides were virtually identical with the respective K_is being 0.31−0.35 nM for **9**, 0.16−0.21 nM for **10**, 0.47 nM for **11**, and 0.17 nM for **12**. On the other hand, the inhibitor **13**, which is an analogue of **15**, was a significantly weaker inhibitor having a K_i of 80 nM.

NMR Structural Studies. Because of the symmetrical nature of the inhibitors **9** and **10**, only a single set of signals corresponding to one molecular half is observed in the ^{1}H NMR spectrum; the notation used to refer to the different signals is shown in Figure 2. The diastereotopic methylene H$^\beta$ protons of the Phe residues at P1/P1′ were assigned using vicinal homonuclear and heteronuclear coupling constants. The detailed ^{1}H and ^{13}C NMR assignments are listed in the Supporting Information.

Solution Structure of 9. No positive cross peaks were detected in the ROESY spectrum of **9**, thereby indicating that it adopted a single major conformation in solution on the NMR shift time scale and that any other conformers were present at concentrations below the limits of detection. A total of 23 distance restraints were obtained from a NOESY spectrum with an S/N of about 400 for geminal peaks, so it was possible to observe H−H distances up to approximately 480 pm. Furthermore, a restraint for the Phe H$^\alpha$−Phe H$^{\alpha'}$ separation was obtained from the ^{13}C satellites of the Phe H$^\alpha$ diagonal peak in a ω_1-^{13}C filtered ROESY spectrum. These two α protons are separated by five bonds, and the chemical shift of Phe H$^\alpha$ (δ, 4.60 ppm) was very close to the applied spinlock frequency of 4.83 ppm, so any TOCSY and NOESY artifact contributions in this restraint are negligible.[23] Because the number of long-range NOEs is small, a reliable conformational analysis is difficult, and special emphasis was therefore placed upon determining a large set of homo- and

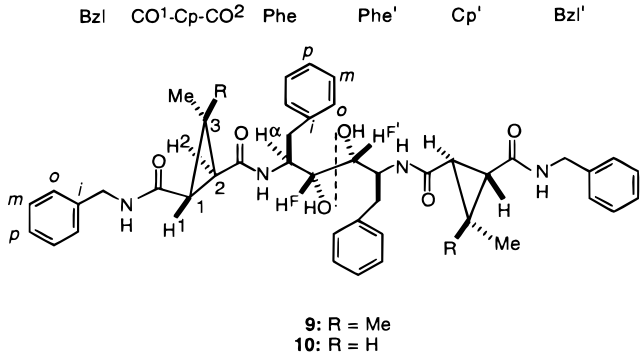

Figure 2. Constitution and conformational labeling in **9** and **10**.

heteronuclear *J* coupling constants.[24] A total of 18 homo- and heteronuclear vicinal *J* values were measured, and the upper limits for two further vicinal *J* values were established.

The orientation of the symmetry center between the 1,2-diol array was determined by the H^F,$H^{F'}$ coupling constant of 10.0 Hz, which was obtained from ^{13}C satellites via a nondecoupled HMQC spectrum (see the Experimental Section); the magnitude of this coupling constant suggests an antiperiplanar arrangement of these protons. Furthermore, the distance between the protons Phe H^{α}—Phe $H^{\alpha'}$ is 2.5 Å, thus indicating that the dihedral angle between the two central C_α carbons is about +60°. Taken together, these observations reliably define the conformation about the carbon—carbon bond of the diol core.

All calculated distance limits were then incorporated as restraints for simulated annealing calculations. The coupling constants for which parameters for the Karplus curves exist were used directly as restraints.[25−27] A total of 21 experimental NOESY distances were set up as 42 symmetry ambiguous restraints of the Nilges type.[28] Because the *J* coupling data rendered two internal NOESY restraints within the Phe residues redundant, these NOESY restraints were not utilized. To maintain the conformation at the symmetry center, the central bond was locked so that the two protons were fixed in an antiperiplanar orientation with the two hydroxyl groups and the two C_α carbons, respectively, being gauche to one another. The simulated annealing procedure converged for **9**, and the conformations of the 12 low-energy structures were very similar having a root-mean-square deviation (rmsd) of <0.6 Å. The lowest energy structure resulting from simulated annealing of **9** was then taken as the starting structure for subsequent molecular dynamic (MD) simulations in DMSO. After 100 ps MD with NOE restraints (±10%, standard pseudoatom correction for upper bounds),[29] the restraints were removed during the following 100 ps MD calculations to determine the stability of the resulting structure. The structure did not change significantly during free MD, suggesting that the resulting rMD structure is energetically favorable. No explicit symmetry forcing was performed during the MD calculations, so the structure displays only approximate C_2 symmetry on this time scale. Figure 3 shows the extended solution structure of **9** that was obtained by

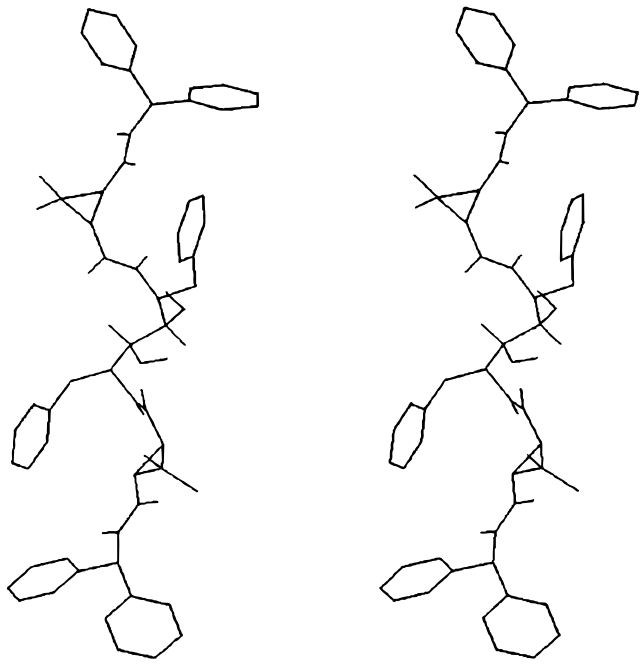

Figure 3. Stereoplot of the structure of **9** obtained by averaging the last 50 ps rMD and subsequent minimization. The terminal Bzl groups do not display a defined orientation in the MD run and were orientated to the two main conformers indicated by *J* coupling data before minimization.

Scheme 4

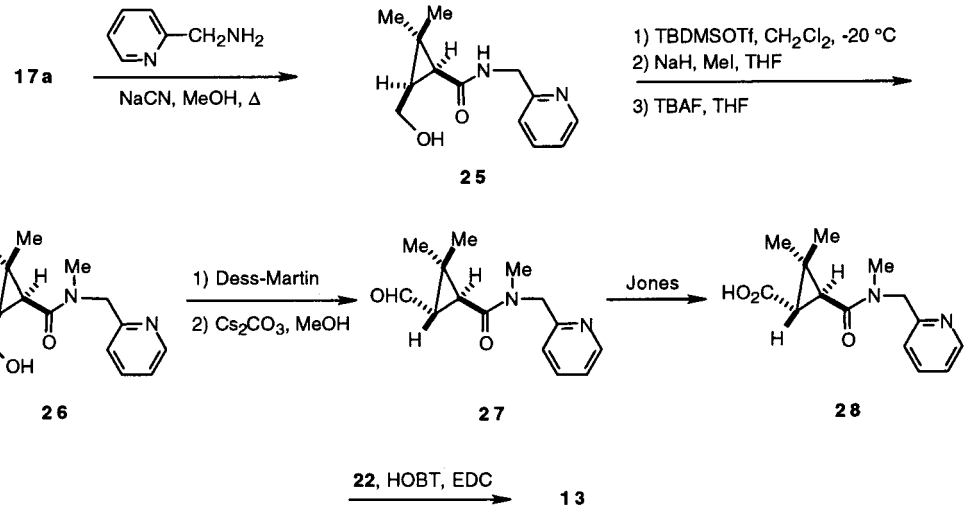

Table 1. Interproton Distances in **9** Determined by ISPA Approximation from a NOESY Spectrum Compared to Distances from the MD Structure (Average during 50 ps rMD)[a]

H_1	H_2[b]	$r_{eff,NOESY}$ (pm)	$r_{eff,MD}$ (pm)	$r_{intra,MD(H1,H2)}$[c] (pm)	$r_{inter,MD(H1,H2')}$[c] (pm)
Bzl H^N	Bzl H^1/Bzl H^2	265	221	221	>1000
Bzl H^N	Cp H^1	229	239	239	>1000
Bzl H^N	Cp H^2	387	422	422	>1000
Cp H^1	Bzl H^1/Bzl H^2	406	412	412	>1000
Cp H^1	Cp Me^{pro-S}	341	266	266	>1000
Cp H^1	Phe H^N	374	317	317	905
Cp H^1	Phe H^α	439	443	452	635
Cp H^2	Cp Me^{pro-R}	332	264	264	>1000
Cp H^2	Phe H^N	224	242	242	802
Cp H^2	Phe H^α	419	444	462	573
Cp H^2	H^F	458	428	598	438
Cp Me^{pro-S}	Phe H^α	417	499	523	629
Cp Me^{pro-S}	Phe $H^{\beta,pro-S}$	350	635	677	769
Cp Me^{pro-S}	H^F	349	598	757	626
Phe H^N	Phe H^α	275	298	302	455
Phe H^N	Phe $H^{\beta,pro-R}$	259	287	288	599
Phe H^N	Phe $H^{\beta,pro-S}$	326	379	388	529
Phe H^N	H^F	303	310	382	328
Phe H^α	Phe $H^{\beta,pro-R}$	303	300	303	482
Phe H^α	Phe $H^{\beta,pro-S}$	270	236	238	402
Phe H^α	H^F	244	244	258	303
Phe H^α	Phe $H^{\alpha'}$	236[d]		–	219
Phe $H^{\beta,pro-R}$	H^F	307	263	265	461
Phe $H^{\beta,pro-S}$	H^F	257	249	249	477

[a] For easy comparison with the NOE data, values in column 4 are the sum of intra and inter symmetric contributions in the MD structure according to $(1/r_{eff})^6 = (1/r_{intra})^6 + (1/r_{inter})^6$. [b] Multiple entries denote integration of an overlapped or degenerate peak; CH_3 peak intensities were divided by 3 before transformation into distances. [c] In cases of degenerate or overlapped peaks the distances were calculated to the corresponding carbon. [d] From ω_1-^{13}C filtered ROESY.

Table 2. Coupling Constants J in **9** in DMSO-d_6 at 300 K[a]

	coupling	J_{exp} (Hz)	J_{MD} (Hz)[g]	$dihedral_{MD}$ (deg)
Bzl	$^3J(H^N, H^1) + {}^3J(H^N, H^2)$	12.0 ± 0.4[b]	–	–
Cp	^3J(Bzl N,H^1)	0.0 ± 0.4[d]	$J(H^{\alpha,15}N_{(i+1)}) = 0.2$	54
	$^3J(CO^1,H^2)$	4.2 ± 1.0[c]	–	9
	$^3J(CO^2,H^1)$	4.3 ± 1.0[c]	–	13
	$^3J(H^1,H^2)$	5.5 ± 0.4[b]	–	148
	$^3J(H^1,C^{Me,pro-S})$	5.0 ± 0.4[d]	–	−6
	$^3J(H^2,C^{Me,pro-R})$	5.2 ± 0.4[d]	–	−9
	^3J(Phe N,H^2)	0.2 ± 0.4[d]	$J(H^{\alpha,15}N_{(i+1)}) = 0.2$	−53
Phe	$^3J(H^N,H^\alpha)$	9.5 ± 0.4[b]	$J(H^N,H^\alpha) = 9.9$	$\Phi = -125$
	$^3J(H^N,C^\beta)$	0.8 ± 0.4[d]	$J(H^N,C^\beta) = 0.2$	$\Phi = -125$
	$^3J(H^N,C^F)$	<0.8[e]	$J(H^N,CO) = 0.8$	$\Phi = -125$
	$^3J(Cp\ CO^2,H^\alpha)$	3.8 ± 1.0[c]	$J(H^\alpha,CO_{(i-1)}) = 2.8$	$\Phi = -125$
	$^3J(H^\alpha,H^{\beta,pro-S})$	3.0 ± 0.4[b]	$J(H^\alpha,H^\beta) = 4.9$	$\chi_1 = -167$
	$^3J(H^\alpha,H^{\beta,pro-R})$	11.0 ± 0.4[b]	$J(H^\alpha,H^\beta) = 11.8$	$\chi_1 = -167$
	$^3J(C^F,H^{\beta,pro-S})$	1.7 ± 1.5[e]	$J(H^\beta,CO) = 0.8$	$\chi_1 = -167$
	$^3J(C^F,H^{\beta,pro\ R})$	1.1 ± 1.5[e]	$J(H^\beta,CO) = 2.1$	$\chi_1 = -167$
	$^3J(H^\alpha,C^i)$	3.3 ± 1.0[c]	–	$\chi_1 = -167$
	$^3J(H^\alpha,H^F)$	<1.0[b]	$J(H^\alpha,H^\beta) = 2.8$	68
	$^3J(H^F,OH)$	5.6 ± 0.4[b]	–	–
	$^3J(H^F,H^{F'})$	9.9 ± 0.4[b]	$J(H^\alpha,H^\beta) = 12.9$	−174

[a] The dihedral J values are compared to J values calculated from the angles in the MD structure (average during 50 ps rMD) using peptidic Karplus curves.[54] [b] From absortive in phase signals. [c] From peak fitting according to Keeler on HMBC and ^{1}H-1D.[50] [d] From heteronuclear E.COSY. [e] From peak intensity simulation-(see Supporting Information). [f] From antiphase signals according to Kim and Prestegaard.[49] [g] Karplus curve parametrization is indicated in parentheses.

averaging the last 50 ps of the rMD followed by minimization; because the terminal Bzl groups did not prefer a defined orientation in the MD run, they are oriented in the two conformers indicated by the J coupling data before minimization.

The structure depicted in Figure 3 is consistent with all of the experimental data (Tables 1 and 2). For example, the observed syn orientations of Phe H^N to Cp H^1 and Cp H^2 to Phe H^N are consonant with the short distances between these protons that were derived from the NMR data. Major violations are recognized only for distances between pseudoatoms. All backbone angles were experimentally determined by at least one distance and at least one three-bond coupling, ^3J, whose value was maximal based upon the Karplus curve; thus, these dihedral angles are well-defined. The extended conformation of the backbone is also in agreement with the observed temperature gradients, which show that the amide protons (Bzl H^N: $d\delta/dT = -5.2$ ppb/K; Phe H^N: $d\delta/dT = -6.0$ ppb/K) are exposed to solvent.[30]

The large sums of the Bzl H^N Bzl H^1 and Bzl H^N Bzl H^2 couplings in the NMR data suggest that the terminal Bzl groups at P3 and P3′ are directed predominantly in the two orientations shown in Figure 3. However, the NMR data also clearly show that these Bzl groups are freely rotating because the Bzl H^1 and Bzl H^2 protons do not show the chemical shift dispersion that would be observed if they resided in a single preferred orientation relative to the preceding Cp CO^1. In contrast, the experimental values of 11 and 3 Hz that were determined for the two ^3J(Phe H^α, Phe H^β) couplings imply that the side chains of Phe and Phe′ have a preferred orientation. Quantitative analysis according to the Pachler equations[31] indicates that the rotamer having $\chi_1 = -60°$ is populated to about 76%, which projects the Phe side chain below the center of the cyclopropane unit. The rotamer $\chi_1 = +60°$ is populated to about 21%. Because of the relatively short simulation time, no interconversion between these rotamers was observed in the MD. The proximity of the phenyl rings of the Phe and Phe′ residues at P1 and P1′ and the cyclopropane units is also suggested by the spatial contacts between the Cp H^1 and H^2 protons and the phenyl protons that were observed in the ROESY spectrum.

Solution Structure of 10. The same protocol used to determine the solution conformation of **9** was applied to the pseudopeptide **10**, but the analysis was compro-

Table 3. Interproton Distances in **10** as Determined by ISPA Approximation from a ROESY Spectrum[a]

H_1[b]	H_2[b]	$r_{eff,ROESY}$ (pm)	$r_{eff,NOESY}$ (**9**) (pm)
Bzl H^N	Bzl H^1/Bzl H^2	246	265
Bzl H^N	Cp H^1/Cp H^2	216	227[c]
Bzl H^N	Cp H^3	514	big[d]
Bzl H^N	Cp H^{Me}	511	big
Cp H^1/Cp H^2	Bzl H^1/Bzl H^2	420	406[c]
Cp H^1/Cp H^2	Cp H^{Me}	311	332[c]
Cp H^1/Cp H^2	Phe H^N	216	222[c]
Cp H^1/Cp H^2	Phe H^α	404	381[c]
Cp H^1/Cp H^2	Phe H^F	402	458[c]
Cp H^3	Bzl H^1/Bzl H^2	553	big[d]
Cp H^3	Phe H^N	457	big[d]
Cp H^3	Phe H^α	421	417[d]
Cp H^3	Phe $H^{\beta1}$/Phe $H^{\beta2}$	401	350[c,d]
Cp H^3	H^F	384	349[d]
Cp H^{Me}	Bzl H^1/Bzl H^2	505	big
Cp H^{Me}	Phe H^N	599	big
Cp H^{Me}	H^F	542	big
Phe H^N	Phe H^α	285	275
Phe H^N	Phe $H^{\beta1}$/Phe $H^{\beta2}$	264	252[c]
Phe H^N	Phe H^F	282	303
Phe H^α	Phe H^F	233	244
Phe $H^{\beta1}$/Phe $H^{\beta2}$	Phe H^F	252	245[c]

[a] For comparison experimental distances between corresponding protons in compound **9** are listed in column 4. [b] Multiple entries denote integration of overlapped or degenerate peak; CH_3 peak intensities were divided by 3. [c] Overlapping in **10** was simulated from corresponding nonoverlapped protons A and B in **9** according to $(1/r_{eff})^6 = (1/r_{PROTON\ A})^6 + (1/r_{PROTON\ B})^6$. [d] Distances from nonequivalent protons are compared: CH_3 versus H.

Table 4. Coupling Constants J in 10 in DMSO-d_6 at 300 K[a]

	coupling	J_{exp} (Hz)	J_{exp} (**9**) (Hz)
Bzl	$^3J(H^N, H^1) + {}^3J(H^N, H^2)$	12.2 ± 0.4[b]	12.0 ± 0.4[b]
Cp	$^3J(CO^1,H^3)$	3.5 ± 1.0[c]	–
	$^3J(CO^2,H^3)$	4.7 ± 1.0[c]	4.3 ± 1.0[c]
	$^3J(H^3,H^1)$	10.0 ± 0.4[b]	–
	$^3J(H^3,H^2)$	5.5 ± 0.4[b]	5.5 ± 0.4[b]
	$^3J(H^3,H^{Me})$	6.0 ± 0.4[b]	–
Phe	$^3J(H^N,H^\alpha)$	9.7 ± 0.4[b]	9.5 ± 0.4[b]
	$^3J(H^N,C^\beta)$	<1.0[d]	0.8 ± 0.4
	$^3J(H^N,C^F)$	<1.0[d]	<0.8[d]
	$^3J(Cp\ CO^2,H^\alpha)$	4.4 ± 1.0[c]	3.8 ± 1.0[c]
	$^3J(H^\alpha,H^{\beta1}) + {}^3J(H^\alpha,H^{\beta2})$	17.2 ± 0.4[b]	–
	$^3J(H^\alpha,C^i)$	3.3 ± 1.0[c]	3.3 ± 1.0[c]
	$^3J(H^\alpha,H^F)$	1.1 ± 0.4[b]	<1.0[b]
	$^3J(H^F,OH)$	5.9 ± 0.4[b]	5.6 ± 0.4[b]
	$^3J(H^F,H^{F'})$	9.8 ± 0.4[b]	9.9 ± 0.4[b]

[a] In the last column, the corresponding experimental J values in compound **9** are listed. [b] From absortive in-phase signals. [c] From peak fitting according to Keeler on HMBC and ^{1}H-1D.[50] [d] From peak intensity simulation.

mised by two factors. First, there was virtually no dispersion for the resonances associated with the cyclopropane protons H^1 and H^2 (1.95 and 1.93 ppm). Second, the Phe H^βs shifts were nearly degenerate (2.68 and 2.64 ppm). A total of 23 ROESY distances were identified that corresponded to H,H distances up to 480 pm, and 14 vicinal J couplings and 2 upper bounds for vicinal J couplings were determined. Tables 3 and 4 list the experimentally determined values with a comparison to the corresponding data for **9**. Examination of these tables reveals the close similarity of the NMR data of **10** and **9**, except for the degeneracies noted above in the spectrum of **10**.

When a simulated annealing procedure was applied to the data for **10**, there was no convergence to a single

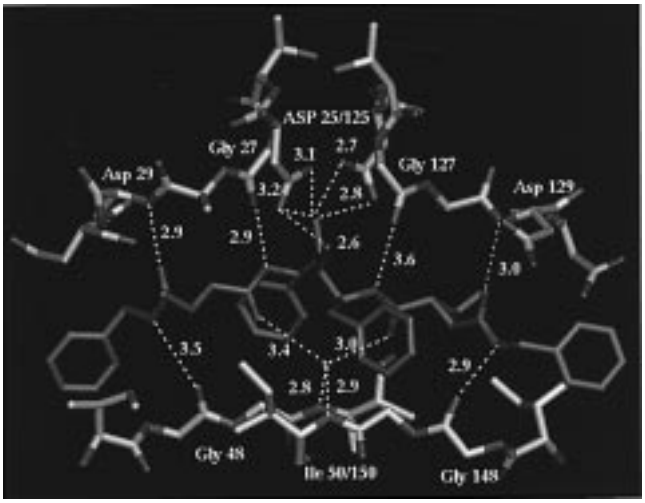

Figure 4. Binding site interactions made by compound **10** and HIV-1 protease observed in the X-ray structure. The inhibitor makes asymmetric interactions with the active site aspartates, Asp25 and 125, as well as with the S and S′ halves of the binding site. Hydrogen bonds are shown as dashed lines with distances in Å. Oxygen and nitrogen atoms are colored red and blue, respectively. Carbon atoms are rust and gray for inhibitor and enzyme, respectively.

Table 5. Refinement Statistics for HIV-1 Protease Complexed with Compound **10**

resolution, Å	7.0−2.0
unique reflections ($\|F\|/\sigma > 2.0$)	6154
completeness	49
R_{merge},[a] %	5.6
R factor, %	18.5
rms bonds, Å	0.013
rms angles, deg	3.1
no. of water molecules	60

[a] $R_{merge} = \sum|I - \langle I\rangle|/\sum I$ where I is the observed intensity and $\langle I\rangle$ is the average intensity obtained from multiple observations. Coordinates will be deposited with the Brookhaven Data Bank.

structure. The failure of these simulated annealing calculations most likely arises from a lack of experimental data, although failure to observe convergence in such calculations may also indicate a flexible molecule for which several conformations are energetically favorable. For example, the absence of distance restraints for the Cp H^1 and CpH^2 protons result in an undefined orientation of the neighboring atom Phe H^N. Because an unbiased starting structure was not obtained, no MD simulations were performed. Nevertheless, the close similarity of the NMR data that was obtained for **9** and **10** indicates that **10** adopts the extended conformation as found for **9** at least part of the time.

Crystallographic Analysis of a Complex of 10 with HIV-1 Protease. The 2.3 Å crystal structure of HIV-1 protease complexed with compound **10** reveals that the inhibitor binds in an extended conformation similar to that found with other peptidomimetic inhibitors of the protease[17b] and with the related C2 symmetry-based inhibitors upon which the design of **10** was based[16d] (Figure 4, Table 5). The two active site aspartic acids of HIV-1 protease are shared unequally by the two OH groups of **10** in a manner characteristic of an asymmetric mode of inhibitor binding in which the molecular 2-fold axis of the enzyme passes close to one of the two hydroxyl-bearing carbon atoms.[16d] One of the hydroxyl groups of **10** is within hydrogen-bonding

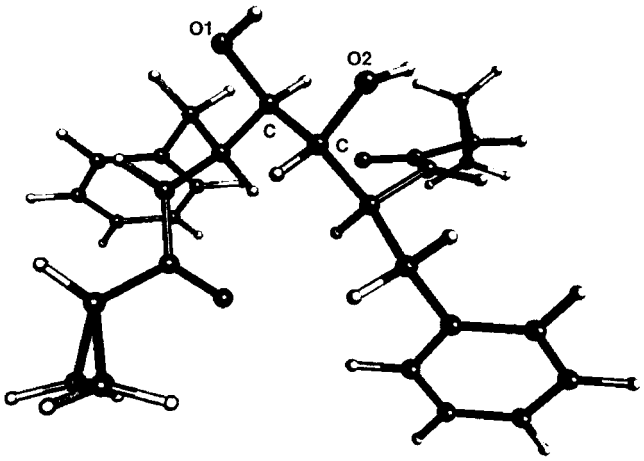

Figure 5. Model of the P2−P2′ portion of compound **12** used for conformational analysis by ab initio methods. Coordinates of the NMR structure of **9** were used to create a starting model which was optimized using DFT methods (see Methods). The structure shown corresponds to the lowest energy conformation (conf 1) listed in Table 6.

Table 6. Relative Energies (kcal/mol) of Optimized Conformations in the Gas Phase (ΔE_g), Calculated Using HF and DFT Methods, and in Water (ΔE_s)[a]

conformation	ΔE_g-HF	ΔE_g-DFT	Θ1 (HF/DFT)	Θ2 (HF/DFT)	ΔE_s
conf 1	0.0	0.0	62.6/61.9	−52.6/−52.6	0.0
conf 2	3.1	1.9	170.2/175.3	55.5/59.9	0.6
conf 3	4.1	4.2	152.2/167.4	32.7/48.3	2.8

[a] The values of torsional angles Θ1 (Cα−C−C−Cα) and Θ2 (O1−C−C−O2) are in degrees.

distance of three of the four aspartate oxygen atoms, whereas that of the other hydroxyl can only hydrogen bond to one aspartate oxygen (Figure 4). The P2 and P2′ carbonyl oxygens make hydrogen bonds with the flap water (Wat 301) that bridges the inhibitor with the enzyme at Ile 50 and 150. However, the inhibitor−Wat 301 hydrogen bond distances are unusually long at 3.4 and 3.0 Å. Similarly the hydrogen bonds between the NH atoms of the P3 and P3′ benzylamides and the Gly48 and Gly148 backbone CO atoms of the enzyme are rather long, being 3.5 and 2.9 Å, respectively.

Conformational Analysis of the Cyclopropanediols. A computational model of the P2−P2′ region of **12** consisting of the 64 atoms (Figure 5) was built using the conformation for the corresponding core region of **9** that was determined by NMR experiments (Figure 3). Rotations of 30° about the central C−C diol bond were performed, and the resulting structures were subjected to complete optimization at an ab initio level of accuracy using Hartree−Fock (HF) and density functional theory (DFT) methods with the 6-31* basis set as implemented in the Gaussian 94 program package.[32−34] This analysis revealed three different structures corresponding to local energy minima in the subspace of torsion angle Θ1 about the central carbon−carbon bond. The relative energies of these conformations and their corresponding torsion angles are shown in Table 6. While some of the parameters listed in Table 6 are sensitive to correlation effects, as shown by the differences between the HF and DFT calculations, good qualitative agreement was obtained using both ab initio methods. The lowest energy conformation (conf 1) is close to the experimental NMR and X-ray crystal structures in the P2−P2′ portion of the inhibitor. The HF- and DFT-optimized structures for conf 1 are nearly identical with rmsd fit for all atoms of 0.12 Å. The torsion angle value calculated for the central dihedral angle Cα−C−C−Cα, Θ1, in conf 1 is within 6° and 16° of the experimentally determined values of 68.1° and 78.6° for the NMR and crystal structures, respectively; these values are well within experimental error. The calculated Θ1 angle for conf 1 is also nearly identical, 61.9−62.6° vs 62.0°, to that found in the related inhibitor **15** with valine at P2 and P2′.[16d] The other two calculated conformational minima, conf 2 and conf 3, have Θ1 angles far outside the range of observed experimental values.

The three optimized conformations also exhibit different hydrogen bonding patterns for the diol hydroxy groups. The relative disposition of the two hydroxyls is given by the torsion angle O1−C−C−O2, Θ2 in Table 6. In the lowest energy structure, conf 1, there is an internal hydrogen between the two hydroxyl groups. In conf 1, Θ2 is −52.6°, compared with −42.5° and −23.4° for the NMR and crystal structures, respectively. In conf 2, one hydroxy group hydrogen bonds to the nitrogen of the closest amide, and the other hydroxy group forms a hydrogen bond with the carbonyl oxygen of the second amide. In conf 3, both hydroxy groups interact with the nitrogen atoms of the nearest amide. These calculations show that the gas phase energy differences between the three structures are determined mainly by differences in the energetics of the hydrogen-bonding patterns. Inclusion of solvation effects reduces these energy differences, but conf 1 is still predicted to be the most stable structure.

Discussion

Numerous X-ray structures of HIV-1 protease complexed with flexible, peptide-derived inhibitors have shown that the inhibitors typically bind to the enzyme active site cleft in an extended, β-strand conformation.[17] On the basis of the working hypothesis that introducing two cyclopropane subunits related to **2** and **3** at the P2 and P2′ subsites of the known HIV-1 protease inhibitors **14** and **15** would stabilize their biologically active conformations, the pseudopeptides **9**−**13** were prepared. The key step in the syntheses of **9**−**13** was an asymmetric, intramolecular cyclopropanation that led to the cyclopropanecarboxylic acids **20a**−**d** and **28**, which were then coupled with the known diamino diol **22** to give the targeted inhibitors **9**−**13**. Each of the pseudopeptides **9**−**13** was found to be a potent, competitive inhibitor of HIV-1 protease in a standard enzyme assay with the K_is being determined as 0.31−0.35 nM for **9**, 0.16−0.21 nM for **10**, 0.47 nM for **11**, 0.17 nM for **12**, and 80 nM for **13**. Although the K_is for **9**−**12** compare favorably with those observed for the related inhibitors **14** (IC_{50} = 0.22 nM) and **15** (K_i = 0.11 nM), **13** was a significantly weaker inhibitor than anticipated.

The structures of the pseudopeptides **9** and **10** in solution were studied to ascertain whether the presence of two cyclopropanes in inhibitors related to **9**−**13** stabilized an extended conformation for the entire ligand. Because of their highly flexible nature, it has generally not been possible to determine the solution structures of linear, peptidomimetic inhibitors for HIV-1

protease. Indeed, prior to the present work, KNI-272, which possesses a central norstatine moiety, was the only such inhibitor whose tight binding was suggested to be partly based on a favorable conformational preorganization of the backbone into the bioactive conformation.[35,36] It is therefore significant that the NMR and associated molecular dynamics investigations conducted with the linear pseudopeptide **9** in DMSO clearly indicate that it adopts a well-defined, preferred conformation in solution in which the backbone is extended (Figure 3). Unfortunately, the lack of sufficient dispersion in the chemical shifts for several key protons in **10** reduced the number of NMR restraints that could be used in simulated annealing calculations, and the available data did not converge to a single structure that could be used in further calculations. Nevertheless, because the NMR parameters that were obtained for **10** correspond well to those measured for **9**, there is good reason to believe that **10** also prefers a similar extended conformation.

A number of factors appear to play roles in stabilizing the extended structure of **9** in solution. Examination of the conformation about the carbon−carbon bond at the symmetry center of the 1,2-diol array reveals an antiperiplanar arrangement of the protons H^F and $H^{F'}$, which is often sterically favored in a tetrasubstituted ethane fragment, and a consequent gauche orientation of the two hydroxyl groups. The preferred gauche orientation of two *vicinal* hydroxyl groups is known,[37] and solvent seems to play a role in stabilizing this conformation.[38] Accordingly the measured temperature gradient ($d\delta/dT = -7.1$ ppb/K) for the proton resonance of the hydroxyl group indicates its exposure to solvent.

To gain further insights regarding the preferred conformational properties about the central core of **9**, ab initio calculations were conducted. Preliminary calculations for a simple model of a C_2 symmetric diol indicated the existence of a large number of interconvertible conformational minima with low-energy barriers.[39] However, such calculations on the cyclopropane-substituted diol segment found in **12** suggest that these rigid backbone replacements at P2 and P2′ can lead to further reduction in conformational flexibility about the otherwise freely rotatable diol core. Thus, the experimentally determined conformation about the central carbon−carbon bond of **9** is the same as that predicted by ab initio calculations and appears to be influenced by the presence of the adjacent cyclopropane rings.

The two dihedral angles that are defined by rotations about the CO^1−Cp C^1 and the Cp C^2−CO^2 bonds in **9** appear to be strongly constrained in an orientation in which there is an approximate synperiplanar arrangement between the Bzl H^N and Cp H^1 protons as well as of the Cp H^2 and Phe H^N protons. This conformation is presumably stabilized by the interaction of the π-orbital of the carbonyl group with the carbon−carbon σ-bond of the adjacent cyclopropane,[40] an arrangement that is found in the solid-state structures of several α,β-cyclopropyl amides.[10] The ϕ-angle of the Phe moiety, which corresponds to rotation about the Phe N^H−Phe Cα bond, is −125°. This conformation is commonly observed in peptides because the syn relationship between the amide carbonyl group and the α-proton minimizes the allylic strain along the extended peptide backbone.[41]

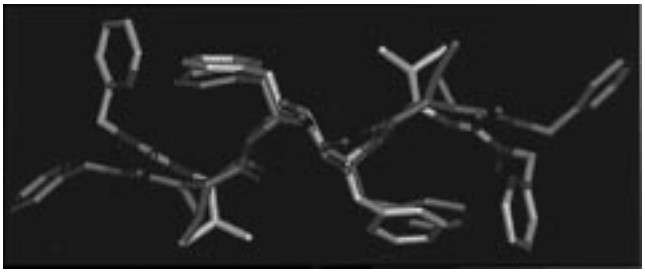

Figure 6. Superposition of inhibitor conformations of compounds **10** (rust-colored) and **15** (A-76889) (gray) complexed with HIV-1 protease. Both compounds adopt very similar conformations near the diol core, but show significant differences in P3−P2 and P2′−P3′. Superposition was performed using only the Cα coordinates for the enzymes from the two complexes (rmsd = 0.7 Å for 198 Ca atoms). Oxygen and nitrogen atoms are colored red and blue, respectively.

The three-dimensional structure of **10** in its complex with HIV-1 protease superimposes well onto the bound conformation of the related inhibitor **15**, particularly in the segment defined by the P2−P2′ moieties (Figure 6). The positions of hydrogen-bonding groups of both inhibitors are spatially conserved throughout their backbones. A comparison of the relative locations of the cyclopropanyl and valinyl side chains of **10** and **15**, respectively, reveals that the methyl substituents of the former nearly overlap with the Cγ methyl groups of their valine counterparts in **15**. Examination of the structure of the complex of **10** with the protease also suggests that both the monomethylated cyclopropane in **11** and the dimethyl-substituted cyclopropane in **9** can fit nicely within the S2 and S2′ enzyme subsites without any significant conformational changes, thereby providing a structural basis for the close similarities in the K_is for the series of inhibitors **9**−**12**. These results are consistent with the initial design principles of these pseudopeptides and support the conclusion that the restrictive cyclopropane moiety can be accommodated within the context of a linear peptidomimetic inhibitor to stabilize an extended conformation.

Despite the structural similarities of the inhibitors **10** and **15** when complexed to HIV-1 protease, there are some notable differences in their specific interactions with the enzyme. Because of the cyclopropane replacements at P2 and P2′, compound **10** lacks the two NH groups that are present in the valinyl residues of **15**. In the complex of **15** with HIV-1 protease, these NH groups form short hydrogen bonds, 3.0 and 3.2 Å, with the corresonding Gly48 and Gly148 backbone CO groups of the enzyme. Interestingly, in the complex of **10** with the protease, the energy lost by the lack of these specific hydrogen bonds is compensated, at least in part, by the formation of two different hydrogen bonds, 3.5 and 2.9 Å, between the NH atoms of the P3 and P3′ benzylamide groups and the respective carbonyl groups of Gly48 and Gly148 (Figure 4).

In the context of considering hydrogen-bonding interactions between the different cyclopropane-derived inhibitors and HIV-1 protease, it is significant that the cyclopropane-derived pseudopeptide **13** lacks not only the valinyl NH groups at the P2 and P2′ subsites of **15** but also the benzylamide NH groups at P3 and P3′ of

9−**12**. Thus, there are no hydrogen bond donors at the P3/P2 and the P3′/P2′ subsites in **13** that can form stabilizing hydrogen bonds with the Gly48 and Gly148 residues of the protease. A comparison of the binding affinities of **13** and **15** suggests that there is an approximately 3.9 kcal difference in their respective binding energies, a value that corresponds approximately to the loss of two hydrogen bonds.[11,12] However, because the presence of *N*-methyl groups at the P3 and P3′ subsites of **13** may also induce other conformational changes arising from their possible interactions with the proximal Cp H^1 and Cp′ H^1 protons, a precise analysis of the basis for the observed difference in binding affinities of **13** and **15** is problematic; additional structural information is required.

Another significant contrast between the crystal structures of the protease complexes of **10** and **15** is in the conformations of the aromatic rings at the P3 and P3′ subsites (Figure 6). In the complex with **15**, the P3/P3′ pyridine rings make electrostatically favorable stacking interactions with the guanidinium groups of Arg8 and Arg108, respectively.[16d] These P3/P3′ pyridine rings in **15** also make hydrogen bonds via the ring nitrogens with water molecules located within the S3 and S3′ pockets.[42] Somewhat surprisingly, another variance in these two complexes is found in the locations of the two central hydroxy groups, which differ by about 1 Å, *despite the identity of the P1*−*P1′* core regions of ***10*** *and* ***15***.

The similarities and differences that are observed between the complexes of **10** and **15** with HIV-1 protease underscore the variable nature of the interactions between small molecule ligands and the active site residues of the protease. The detailed binding mode for a given inhibitor is a consequence of optimizing many different interactions within the relatively large and flexible binding site. Because **10** and **15** are virtually equipotent inhibitors of HIV-1 protease, the overall energetics of their binding to the enzyme are approximately equal, the changes in one specific interaction being balanced by another factor.

The averaged and energy-minimized structure of **9** in DMSO as determined from rMD calculations using NMR restraints is very similar to the three-dimensional structure of the bound form of **10** as obtained from X-ray analysis of its complex with HIV-1 protease (Figure 7). This structural similarity suggests that there may little entropy loss on binding of these and related ligands to the protease. The structures of **9** and **10** are most closely conserved in the conformations of their diol cores, which superimpose to within 0.15 Å rmsd. The side chain phenyl groups at P1 and P1′ in both the solution and solid-state structures are oriented in the gauche-(−) conformation with $\chi_1 = -60°$. Although there is also good similarity in the structures of the two inhibitors in the P2 and P2′ regions containing the cyclopropane replacements, there are significant differences in the conformations of the P3 and P3′ subsites. In the solution structure of compound **9**, the P3/P3′ benzyl groups are freely rotating, whereas in the bound structure of **10**, the P3 and P3′ groups are oriented toward the P2 and P2′ cyclopropyl groups. If the solution and bound conformations of **9** and **10** are similar, then binding of these pseudopeptides to the HIV-1 protease will require restriction of the torsional flexibility at the P3 and P3′ subsites; however, the similar K_i values for the two compounds suggest that the conformational adjustments required for binding are probably comparable.

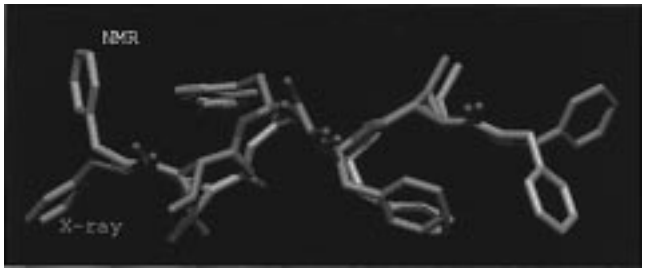

Figure 7. Comparison of crystal structure of compound **10** (rust-colored) complexed with HIV-1 protease with an averaged, minimized structure of compound **9** (gray) in solution as determined by NMR. In the solution structure of **9**, the benzyl groups at P3 and P3′ are disordered in the NMR structure as indicated by the stippled dot surfaces. Coordinates for six pairs of atoms in the diol core portions of the two inhibitors were used for the superposition analysis (rmsd = 0.15 Å). Oxygen and nitrogen atoms are colored red and blue, respectively.

Conclusion

As part of a general program directed toward the de novo design of molecules having defined topographical and biological properties, the pseudopeptides **9**−**13** were prepared as potential inhibitors of HIV-1 protease. The design of these targets was based upon the hypothesis that the presence of two cyclopropane rings, which are *N*-terminal truncated analogues of the dipeptide mimics **2** and **3**, at the P2 and P2′ subsites of **9**−**13** would stabilize the biologically active conformations of the related HIV-1 protease inhibitors **14** and **15**. The results presented herein provide compelling evidence supporting this hypothesis. The similarity of K_i values for the different cyclopropane analogues **9**−**12** suggests that small substituents at the 2-position of the cyclopropane ring do not adversely affect the relative stability of the bioactive conformation of the inhibitor. This conclusion is supported both by the NMR data, which are similar for **9** and **10**, and by the model calculations that were done using the unsubstituted analogue **12**. The magnitude of the reduced affinity of **13** was unexpected and presumably results from a combination of undetermined conformational factors at the P3/P3′ subsites coupled with a reduced hydrogen bonding capability. The combination of NMR and X-ray structural work with the HIV-1 protease inhibitors **10** and **9**, respectively, indicates that the preferred solution conformation of these inhibitors corresponds closely to their structure when bound to the protease active site. These results further suggest that the cyclopropane-derived peptidomimetics found in **9**−**12** stabilize and enforce a three-dimensional structure at the P2/P1 and P2′/P1′ positions that corresponds closely to the biologically active conformation at the same subsites of the HIV-1 protease inhibitors **14** and **15**. Despite the similarities of the bound structures of **10** and **15** within the protease active site, there are some significant differences in the specific enzyme/inhibitor interactions that result from the optimization of many interactions

within a relatively large and flexible binding site, and the results of such investigations will be reported in due course. With this caveat in mind, substituted cyclopropanes might be used to probe structure−activity relationships of S2 and S2′ subsite preferences.

Experimental Section

Unless otherwise noted, solvents and reagents were reagent grade and used without purification. Tetrahydrofuran (THF) was distilled from potassium/benzophenone ketyl under nitrogen, and dichloromethane (CH_2Cl_2) was distilled from calcium hydride prior to use. Reactions involving air or moisture sensitive reagents or intermediates were performed under an inert atmosphere of argon in glassware that had been oven or flame dried. Melting points are uncorrected. Infrared (IR) spectra were recorded either neat on sodium chloride plates or as solutions in $CHCl_3$ as indicated and are reported in wavenumbers (cm^{-1}) referenced to the 1601.8 cm^{-1} absorption of a polystyrene film. ^1H (300 MHz) and ^{13}C (75.5 MHz) NMR spectra were obtained as solutions in $CDCl_3$ unless otherwise indicated, and chemical shifts are reported in parts per million (ppm, δ) downfield from internal standard Me_4Si (TMS). Coupling constants are reported in hertz (Hz). Spectral splitting patterns are designated as s, singlet; br, broad; d, doublet; t, triplet; q, quartet; m, multiplet; and comp, complex multiplet. Flash chromatography was performed using Merck silica gel 60 (230−400 mesh ASTM). Percent yields are given for compounds that were ≥95% pure as judged by NMR.

[1*S*-(1α,2α)]-(*N*-Benzyl-*N*-*p*-methoxybenzyl)-2-(hydroxymethyl)-3,3-dimethylcyclopropane-1-carboxamide (18a). A 2.0 M solution of Me_3Al in hexanes (1.2 mL, 2.4 mmol) was slowly added to a suspension of *N*-benzyl-*N*-(4-methoxybenzyl)amine (0.54 g, 2.4 mmol) in 1,2-dichloroethane (DCE) (8 mL). The reaction mixture was stirred at room temperature for 30 min, whereupon a solution of the cyclopropyl lactone **17a**[19c] (150 mg, 1.2 mmol) in DCE (0.5 mL) was slowly added. The reaction was refluxed for 24 h, cooled to 0 °C, and carefully quenched with 1 N HCl (4 mL). The reaction mixture was extracted with CH_2Cl_2 (3 × 10 mL), dried ($MgSO_4$), and concentrated under reduced pressure. The crude product thus obtained was purified by flash chromatography eluting with hexanes/EtOAc (1:1) to give 318 mg (75%) of **18a** as a colorless oil: ^1H NMR (rotamers) δ 7.40−7.05 (comp, 7 H), 6.92 (d, J = 8.6 Hz, 1 H), 6.84 (d, J = 8.6 Hz, 1 H), 5.21 and 5.16 (rotameric d, J = 14.6 Hz, 1 H), 4.75 and 4.70 (rotameric d, J = 16.6 Hz, 1 H), 4.29 and 4.24 (rotameric d, J = 16.6 Hz, 1 H), 4.16−3.87 (comp, 3 H), 3.83 and 3.80 (rotameric s, 3 H), 1.64 and 1.60 (rotameric d, J = 8.5 Hz, 1 H), 1.41−1.31 (m, 1 H), 1.15 and 1.14 (rotameric s, 3 H), 1.12 and 1.11 (rotameric s, 3 H); ^{13}C NMR (rotamers) δ 172.1, 159.0, 158.5, 133.5, 133.0, 129.5, 128.9, 128.5, 128.1, 127.8, 127.6, 127.3, 126.4, 114.3, 113.9, 59.4, 55.2, 55.1, 49.8, 49.4, 47.5, 47.1, 31.9, 30.4, 27.6, 23.7, 15.9; IR ($CHCl_3$) ν 3457, 2948, 1628 cm^{-1}; mass spectrum (CI) m/z 354.2060 ($C_{22}H_{29}N_1O_3$ + H requires 354.2069), 336.

[1*R*-(1α,2α,3α)]-(*N*-Benzyl-*N*-*p*-methoxybenzyl)-2-(hydroxymethyl)-3-methylcyclopropane-1-carboxamide (18b). Prepared as a colorless oil in 75% yield from **17b** after purification flash chromatography eluting with hexanes/EtOAc (1:1) according to procedure described for **18a**: ^1H NMR (rotamers) δ 7.40−7.09 (comp, 7 H), 6.91 (d, J = 8.7 Hz, 1 H), 6.83 (d, J = 8.7 Hz, 1 H), 5.20 (d, J = 14.4 Hz, 1 H), 4.99 and 4.83 (rotameric d, J = 16.6 Hz, 1 H), 4.32 and 4.27 (rotameric d, J = 16.6 Hz, 1 H), 4.10−3.84 (comp, 3 H), 3.81 and 3.79 (rotameric s, 3 H), 1.87 and 1.82 (rotameric t, J = 8.8 Hz, 1 H), 1.58−1.41 (comp, 2 H), 1.14 and 1.11 (rotameric d, J = 7.0 Hz, 3 H); ^{13}C NMR (rotamers) δ 171.8, 159.0, 158.9, 137.1, 136.2, 129.5, 129.2, 128.9, 128.5, 128.1, 127.8,127.6, 126.4, 114.4, 113.9, 58.7, 55.3, 55.2, 49.7, 49.4, 47.6, 47.2, 23.9, 22.6, 17.0, 16.9, 9.2, 9.1; IR ($CDCl_3$) ν 3407, 2955, 1614, 1512, 1467, 1248, 1032 cm^{-1}; mass spectrum (CI) m/z 340.1913 ($C_{21}H_{25}NO_3$ + H requires 340.1922).

[1*R*-(1α,2α)]-(*N*-Benzyl-*N*-*p*-methoxybenzylaminylcarbonyl)-2-formyl-3,3-dimethylcyclopropane-1-carboxamide. A solution of the alcohol **18a** (166 mg, 0.47 mmol) and pyridinium chlorochromate (PCC) (199 mg, 0.94 mmol) dissolved in dry CH_2Cl_2 (10 mL) was stirred for 12 h at room temperature. The mixture was then diluted with Et_2O (10 mL) and filtered through a small plug of silica gel. The solvent was concentrated under reduced pressure, and the crude material was purified by flash chromatography eluting with hexanes/EtOAc (1:1) to afford 148 mg (93%) of the aldehyde as a clear oil: ^1H NMR (rotamers) δ 9.70 (d, J = 8.6 Hz, 1 H), 7.40−7.05 (comp, 7 H), 6.92 (dd, J = 8.6 Hz, 1 H), 6.85 (d, J = 8.6 Hz, 1 H), 5.02 and 4.95 (rotameric d, J = 14.4 Hz, 1 H), 4.63 and 4.60 (rotameric d, J = 16.6 Hz, 1 H), 4.44 and 4.35 (rotameric d, J = 14.4 Hz, 1 H), 4.20 and 4.15 (rotameric d, J = 16.6 Hz, 1 H) 3.80 and 3.78 (rotameric s, 3 H), 2.32 and 2.27 (rotameric d, J = 8.7 Hz, 1 H), 2.79 and 2.75 (rotameric t, J = 8.7 Hz, 1 H), 1.49 and 1.47 (rotameric s, 3 H), 1.18 and 1.11 (rotameric s, 3 H); ^{13}C NMR (rotamers) δ 200.7, 169.6, 159.5, 159.4, 136.7, 136.5, 129.6, 129.0, 128.6, 128.2, 127.6, 126.3, 114.4, 114.0, 55.1, 55.0, 50.0, 49.0, 48.1, 48.0, 39.9, 39.5, 29.2, 28.6, 28.5, 15.6, 15.5; IR ($CHCl_3$) ν 2955, 1701, 1647 cm^{-1}; mass spectrum (CI) m/z 352.1922 ($C_{22}H_{25}N_1O_3$ + H requires 352.1912), 260, 121.

[1*R*-(1α,2*β*)-(*N*-Benzyl-*N*-*p*-methoxybenzylaminylcarbonyl)-2-formyl-3,3-dimethylcyclopropane-1-carboxamide (19a). The aldehyde from the preceding experiment (100 mg, 0.30 mmol) was dissolved in degassed MeOH (10 mL) containing K_2CO_3 (151 mg, 1.08 mmol), and the reaction was stirred for 24 h at room temperature. Water (10 mL) was added, and the mixture was extracted with CH_2Cl_2 (3 × 30 mL). The combined organic extracts were dried ($MgSO_4$) and concentrated under reduced pressure to afford 80 mg (80%) of **19a** as a clear viscous oil; ^1H NMR (rotamers) δ 9.70 and 9.69 (rotameric d, J = 7.4 Hz, 1 H), 7.41−7.05 (comp, 7 H), 6.90 (d, J = 8.6 Hz, 1 H), 6.84 (d, J = 8.6 Hz, 1 H), 4.85 and 4.83 (rotameric d, J = 15.2 Hz, 1 H), 4.62 and 4.58 (rotameric d, J = 15.2 Hz, 1 H), 4.46−4.28 (comp, 2 H), 3.81 and 3.79 (rotameric s, 3 H), 2.77−2.75 (m, 1 H), 2.61 and 2.55 (rotameric d, J = 5.0 Hz, 1 H), 1.26 and 1.23 (rotameric s, 3 H), 1.14 and 1.07 (rotameric s, 3 H); ^{13}C NMR (rotamers) δ 199.4, 169.1, 158.8, 158.7, 137.8, 137.2, 129.6, 129.4, 129.0, 128.6, 128.2, 127.7, 127.5, 127.1, 126.4, 114.4, 113.9, 55.2, 55.1, 49.6, 49.5, 48.2, 48.1, 40.3, 35.3, 33.0, 21.0, 20.9, 20.0, 19.9; IR ($CHCl_3$) ν 2970, 1710, 1646 cm^{-1}; mass spectrum (CI) m/z 352.1922 ($C_{22}H_{25}N_1O_3$+H requires 352.1912), 260.

[1*R*-(1α,2α,3α)]-(*N*-Benzyl-*N*-*p*-methoxybenzylaminylcarbonyl)-2-formyl-3-methylcyclopropane-1-carboxamide. Prepared from **18b** as a clear glass in 88% yield using the procedure described for the oxidation of **18a**: ^1H NMR (rotamers) δ 9.85 (d, J = 5.9 Hz, 1 H), 7.38−7.09 (comp, 7 H), 6.91 (d, J = 8.5 Hz, 1 H), 6.85 (d, J = 8.5 Hz, 1 H), 5.04 and 4.99 (rotameric d, J = 14.7 Hz, 1 H), 4.72 and 4.68 (rotameric d, J = 16.7 Hz, 1 H), 4.43 and 3.38 (rotameric d, J = 16.7 Hz, 1 H), 4.21−4.10 (m, 1 H), 3.82 and 3.80 (rotameric s, 3 H), 2.52 and 2.46 (rotameric t, J = 8.9 Hz, 1 H), 1.92−1.77 (comp, 2 H), 1.51 and 1.48 (rotameric d, J = 6.5 Hz, 3 H); ^{13}C NMR (rotamers) δ 200.4, 168.9, 159.3, 137.1, 136.2, 129.7, 129.1, 129.0, 128.6, 128.2, 127.8, 127.7, 127.6, 127.5, 126.3, 114.4, 114.0, 55.4, 55.3, 50.2, 50.0, 48.5, 48.1, 31.9, 31.1, 21.4, 21.3, 21.0, 14.2, 9.0; IR ($CDCl_3$) ν 2934, 1696, 1636, 1512, 1248, 1204, 1175, 1036 cm^{-1}; mass spectrum (CI) m/z 338.1756 ($C_{21}H_{23}NO_3$ + H requires 338.1748), 324, 266, 230, 154, 137, 121.

[1*R*-(1α,2*β*,3α)]-(*N*-Benzyl-*N*-*p*-methoxybenzylaminylcarbonyl)-2-formyl-3-methylcyclopropane-1-carboxamide (19b). Prepared from the preceding aldehyde as a clear glass in 91% yield using the procedure described for the preparation of **19a**: ^1H NMR (rotamers) δ 9.59 and 9.58 (rotameric d, J = 8.2 Hz, 1 H), 7.39−7.08 (comp, 7 H), 6.90 (d, J = 8.5 Hz, 1 H), 6.84 (d, J = 8.5 Hz, 1 H), 4.96 and 4.91 (rotameric d, J = 14.7 Hz, 1 H), 4.74 and 4.69 (rotameric d, J = 16.8 Hz, 1 H), 4.42 and 4.37 (rotameric d, J = 16.3 Hz, 1 H), 4.25 and 4.19 (rotameric d, J = 14.7 Hz, 1 H), 3.81 and 3.79 (rotameric s, 3 H), 2.75−7.71 (m, 1 H), 2.61 and 2.55

(rotameric dd, J = 4.4, 9.6 Hz, 1 H), 1.89−1.81 (m, 1 H), 1.22 and 1.20 (rotameric d, J = 6.3 Hz, 3 H); ^{13}C NMR (rotamers) δ 199.7, 167.9, 159.1, 137.1, 136.2, 129.6, 129.1, 128.9, 128.5, 128.1, 127.9, 127.8, 127.6, 127.4, 126.4, 114.2, 113.9, 55.3, 55.1, 49.6, 49.3, 48.3, 48.0, 35.7, 29.7, 24.8, 24.7, 11.7, 11.6; IR ($CDCl_3$) ν 2934, 1702, 1627, 1513, 1464, 1284, 1213, 1175, 1035 cm^{-1}; mass spectrum m/z 338.1756 ($C_{21}H_{23}NO_3$ + H requires 338.1752), 324, 233, 175.

[1*R*-(1α,2*β*)]-(*N*-Benzyl-*N*-*p*-methoxybenzyl)-2-carboxyl-3,3-dimethylcyclopropane-1-carboxamide. A solution of 8 N Jones reagent (4 equiv) was added to a stirred solution of **19a** (100 mg, 0.28 mmol) in acetone (2.8 mL) at 0 °C, and the reaction was stirred for 3 h. Aqueous 1 N HCl (3 mL) was added, and the mixture was extracted with CH_2Cl_2 (3 × 10 mL). The combined organic layers were dried ($MgSO_4$) and concentrated under reduced pressure, and the crude acid was purified by flash chromatography eluting with hexanes/EtOAc (1:1) containing 2% AcOH to afford 97 mg (93%) of the carboxylic acid as a white solid: mp 165−167 °C; ^{1}H NMR (rotamers) δ 7.40−7.01 (comp, 7 H), 6.90 (d, J = 8.6 Hz H), 6.81 (d, J = 8.6 Hz, 1 H), 4.88 and 4.80 (rotameric d, J = 16.3 Hz, 1 H), 4.62 and 4.55 (rotameric d, J = 16.3 Hz, 1 H), 4.21−4.15 (comp, 2 H), 3.80 and 3.78 (rotameric s, 3 H), 2.44 and 2.41 (rotameric d, J = 6.0 Hz, 1 H), 2.38 and 2.32 (rotameric d, J = 6.0 Hz, 1 H), 1.15 (comp, 6 H); ^{13}C NMR (rotamers) δ 176.5, 169.1, 159.2, 159.0, 137.2, 136.5, 129.6, 129.2, 128.9, 128.6, 128.5, 128.1, 127.9, 127.7, 129.4, 126.5, 114.4, 113.9, 55.3, 49.8, 49.5, 48.1, 48.0, 34.9, 31.6, 30.5, 20.8, 19.8, 19.7; IR ($CHCl_3$) ν 2957, 2622, 1731 cm^{-1}; mass spectrum (CI) m/z 368.1858 ($C_{22}H_{25}N_1O_4$+H requires 368.1861), 349, 322, 136, 121.

[1*R*-(1α,2*β*)]-(*N*-Benzyl)-2-carboxyl-3,3-dimethylcyclopropane-1-carboxamide (20a). The (*N*-benzyl-*N*-*p*-methoxybenzyl)-2-carboxyl-3,3-dimethylcyclopropane-1-carboxamide from the preceding experiment (200 mg, 0.810 mmol) was dissolved in trifluoroacetic acid (TFA) (10 mL), and the solution was stirred for 24 h at room temperature. The reaction mixture was concentrated under reduced pressure, and the residue was dissolved in CH_2Cl_2 (50 mL). The organic layer was washed with water (2 × 25 mL), dried ($MgSO_4$), and concentrated under reduced pressure to leave a yellow solid that was purified by flash chromatography eluting with hexanes/EtOAc (1:1) containing 2% AcOH to give 180 mg (90%) of **20a** as a white solid: mp 178−180 °C; ^{1}H NMR δ 7.40−7.29 (comp, 5 H), 6.40 (t, J = 2.8 Hz, 1 H), 4.41 (d, J = 5.7 Hz, 2 H), 2.32 (d, J = 5.6 Hz, 1 H), 2.06 (d, J = 5.6 Hz, 1 H), 1.32 (s, 3 H), 1.25 (s, 3 H); ^{13}C NMR δ 176.0, 168.7, 138.0, 128.7, 127.5, 127.3, 126.7, 126.5, 43.8, 35.9, 32.1, 30.5, 20.5, 20.3; IR ($CHCl_3$) ν 2954, 2750, 1697, 1649 cm^{-1}; mass spectrum (CI) m/z 268.2528 ($C_{14}H_{17}N_1O_3$ + H requires 268.2532), 248(M+1), 230, 202, 184, 141, 91.

[1*R*-(1α,2*β*,3α)]-(*N*-Benzyl-*N*-*p*-methoxybenzylaminyl-carbonyl)-2-carboxyl-3-methylcyclopropane-1-carboxamide. Prepared as a yellow oil in 94% yield from the aldehyde **19b** using the procedure described for the oxidation of **19a**: ^{1}H NMR δ 10.00−9.40 (br s, 1 H), 7.39−7.08 (comp, 7 H), 6.90 (d, J = 8.6 Hz, 1 H), 6.83 (d, J = 8.6 Hz, 1 H), 4.93 and 4.90 (rotameric d, J = 14.7 Hz, 1 H), 4.73 and 4.70 (rotameric d, J = 16.4 Hz, 2 H), 4.42 and 4.36 (rotameric d, J = 16.4 Hz, 1 H), 4.26 and 4.20 (rotameric d, J = 14.7 Hz, 1 H), 3.80 and 3.79 (rotameric s, 3 H), 2.52 and 2.47 (rotameric dd, J = 4.5, 9.7 Hz, 1 H), 2.40−2.36 (m, 1 H), 1.83−1.74 (m, 1 H), 1.19 and 1.17 (rotameric d, J = 6.5 Hz, 3 H); ^{13}C NMR (rotamers) δ 178.2, 168.4, 159.1, 159.0, 137.1, 136.2, 129.6, 129.1, 128.9, 128.7, 128.2, 127.9, 127.7, 127.4, 126.6, 114.4, 114.0, 55.3, 55.2, 49.7, 49.4, 48.2, 47.9, 29.2, 26.7, 24.2, 24.1, 20.6, 11.7, 11.6; IR ($CDCl_3$) ν 3412, 3025, 1519, 1419, 1208 cm^{-1}; mass spectrum (CI) m/z 354.1705 ($C_{21}H_{23}NO_4$ + H requires 354.1709), 262, 154, 136, 121, 107.

[1*R*-(1α,2*β*,3α)]-(*N*-Benzyl)-2-carboxyl-3-methylcyclopropane-1-carboxamide (20b). Prepared as a white solid in 77% yield from the carboxylic acid in the preceding experiment using the procedure described for the preparation of **20a**: mp 150−152 °C; ^{1}H NMR (CD_3OD) δ 7.33−7.20 (comp, 5 H), 4.40 (d, J = 15.0 Hz, 1 H), 4.34 (d, J = 15.0 Hz, 1 H), 2.24 (dd, J = 5.0, 9.6 Hz, 1 H), 2.01 (dd, J = 5.0, 10.1 Hz, 1 H), 1.75−1.68 (m, 1 H), 1.20 (d, J = 6.3 Hz, 3 H); ^{13}C NMR (CD_3OD) δ 176.2, 170.9, 140.0, 129.5, 128.5, 128.2, 44.3, 30.7, 27.7, 24.2, 11.5; IR (Nujol) ν 3370, 2937, 2498, 1697, 1650, 1459, 1122, 977 cm^{-1}; mass spectrum (CI) m/z 234.1130 ($C_{13}H_{15}NO_3$ + H requires 234.1139), 151.

[1*R*,2*S*]-1-[4-(2′-Aminomethylpyridine)-carbonyl]-2-(hydroxymethyl)-3,3-dimethylcyclopropane (25). A solution containing the lactone **17a** (50 mg, 0.4 mmol), 2-aminomethyl pyridine (0.25 mL, 2.4 mmol), catalytic NaCN (2 mg, 0.04 mmol), and MeOH (1 mL) was heated in a sealed flask at 70 °C for 72 h. The solvent was removed under reduced pressure, and the crude orange-red oil was purified via flash chromatography eluting with MeOH/CH_2Cl_2 (5:95) to give 92 mg (98%) of **25** as an amber oil: ^{1}H NMR δ 8.54 (d, J = 4.7 Hz, 1 H), 7.74 (dt, J = 1.7, 7.7 Hz, 1 H), 7.67 (dd, J = 5.8, 16.3 Hz, 1 H), 7.50 (dd, J = 4.9, 16.3 Hz), 4.67 (dd, J = 5.8, 16.3 Hz, 1 H), 4.50 (dd, J = 4.9, 16.3 Hz, 1 H), 4.12 (br s, 1 H), 3.98 (dd, J = 6.4, 12.1 Hz, 1 H), 3.82 (dd, J = 9.8, 12.1 Hz, 1 H), 1.54 (d, J = 8.7 Hz, 1 H), 1.39 (ddd, J = 6.4, 8.7, 9.8 Hz, 1 H), 1.19 (s, 3 H), 1.18 (s, 3 H); ^{13}C NMR δ 171.7, 157.3, 150.0, 136.9, 122.6, 59.4, 52.8, 36.1, 34.0, 32.1, 28.0, 23.5, 15.9; IR ($CDCl_3$) ν 3440, 3054, 1648, 1512, 1422, 1265 cm^{-1}; mass spectrum (CI) m/z 235.1447 ($C_{13}H_{18}N_2O_2$ + H requires 235.1438) 217, 203, 154, 135, 109.

[1*R*,2*S*]-1-[4-(2′-Aminomethylpyridine)carbonyl]-2-(*tert*-butyldimethylsilyloxymethyl)-3,3 dimethylcyclopropane. A solution of the alcohol **25** (812 mg, 3.47 mmol) in CH_2Cl_2 (17 mL) was cooled to −20 °C, and TBDMS triflate (1.15 mL, 6.93 mmol) and 2,6-lutidene (0.92 mL, 5.21 mmol) were added sequentially. The cooling bath was removed, and the reaction was stirred for 1 h. Saturated $NaHCO_3$ (10 mL) was added, and the layers were separated. The aqueous phase was then extracted with CH_2Cl_2 (3 × 10 mL), and the combined organics were dried ($MgSO_4$), concentrated, and purified via flash chromatography, eluting with MeOH/CH_2Cl_2 (3:97) to give 1.083 g (90%) of the TBDMS protected alcohol as a tan oil: ^{1}H NMR δ 8.52 (ddd, J = 0.8, 1.7, 4.9 Hz, 1 H), 7.64 (dt, J = 1.7, 7.7 Hz, 1 H), 7.30−7.19 (comp, 2 H), 7.18−7.15 (m, 1 H), 4.54 (d, J = 5.3 Hz, 1 H), 4.53 (d, J = 5.3 Hz, 1 H), 4.10 (dd, J = 7.2, 11.3 Hz, 1 H), 3.88 (dd, J = 7.7, 11.3 Hz, 1 H), 1.45 (d, J = 8.9 Hz, 1 H), 1.27−1.22 (m, 1 H), 1.24 (s, 3 H), 1.17 (s, 3 H), 0.86 (s, 9 H), 0.05 (s, 3 H), 0.02 (s, 3 H); ^{13}C NMR δ 170.5, 157.2, 148.9, 148.8, 136.6, 122.1, 121.8, 59.4, 44.6, 32.7, 31.2, 28.8, 25.9, 25.8, 22.9, 18.1, 14.9; IR ($CDCl_3$) ν 3308, 2955, 2857, 1654, 1508, 1256, 1072, 836 cm^{-1}; mass spectrum (CI) 349.2311 ($C_{19}H_{32}N_2O_2Si$ + H requires 349.2305) 333, 291, 247, 231, 217.

[1*R*,2*S*]-1-[4-(2′-(*N*-Methyl)aminomethylpyridine)carbonyl]-2-(*tert*-butyldimethylsilyloxymethyl)-3,3-dimethylcyclopropane. To a suspension of NaH (35% dispersion in oil, 31 mg, 1.28 mmol) in THF (0.6 mL) at 0 °C was added the preceding TBDMS protected alcohol (110 mg, 0.32 mmol) in a small amount of THF (0.1 mL). This mixture was stirred for 15 min, whereupon methyl iodide (0.08 mL, 1.28 mmol) was slowly added and the heterogeneous mixture was stirred for 2 h. Water (4 mL) and ether were then added, and the layers were separated. The aqueous phase was extracted with ether (3 × 2 mL), and the combined organics were dried ($MgSO_4$), concentrated, and purified via flash chromatography, eluting with MeOH/CH_2Cl_2 (1:99) to give 96 mg (83%) of the *N*-methyl TBDMS protected alcohol as an orange oil: ^{1}H NMR (rotamers) δ 8.59 & 8.52 (rotameric d, J = 4.0 Hz, 1 H), 7.71 and 7.63 (rotameric dt, J = 1.7, 7.7 Hz, 1 H), 7.30−7.14 (comp, 2 H), 4.77−4.60 (m, 2 H), 4.09−3.90 (m, 2H), 3.10 and 2.99 (rotameric s, 3 H), 1.58 and 1.51 (rotameric d, J = 9.0 Hz, 1 H), 1.30−1.08 (comp, 7 H), 0.89 (s, 9 H), 0.05 (s, 6 H); ^{13}C NMR (rotamers) δ 171.6, 171.0, 157.7, 157.4, 149.7, 149.0, 136.7, 122.3, 122.0, 121.7, 120.1, 60.0, 59.8, 55.6, 52.7, 35.8, 34.2, 33.1, 32.5, 29.8, 28.9, 28.4, 26.4, 25.9, 25.4, 23.0, 22.3, 18.1, 15.1, 14.9; IR ($CDCl_3$) ν 3424, 2955, 2857, 1636, 1472, 1436, 1403, 1257, 1075 cm^{-1}; mass spectrum (CI) m/z 363.2467 ($C_{20}H_{34}N_2O_2$-Si + H requires 363.2472) 347, 305, 231, 217, 149, 123.

[1*R*,2*S*]-1-[4-(*N*-Methyl)aminomethylpyridine)carbonyl]-2-(hydroxymethyl)-3,3-dimethylcyclopropane (26). To a solution of the preceding *N*-methyl TBDMS protected alcohol (302 mg, 0.83 mmol) in THF (5 mL) at 0 °C was added TBAF (1.5 mL, 1.50 mmol), and the mixture was stirred for 2.5 h at 0 °C. Saturated $NaHCO_3$ (5 mL) was added, and the mixture was extracted with Et_2O (3 × 10 mL). The combined organic layers were dried ($MgSO_4$) and concentrated, and the residue was purified by flash chromatography, eluting with MeOH/CH_2Cl_2 (2:98) to give 209 mg (96%) of **26** as an amber oil: ^{1}H NMR (rotamers) δ 8.60 and 8.52 (rotameric d, J = 4.8 Hz, 1H), 7.73 and 7.66 (rotameric dt, J = 1.7, 7.7 Hz, 1 H), 7.28−7.17 (m, 2 H), 5.00 (rotamer, d, J = 15.3 Hz, 0.5 H), 4.78 and 4.68 (rotameric d, J = 17.0 Hz, 1 H), 4.50 (rotamer, d, J = 15.3 Hz, 0.5 H), 3.94 (rotameric d, J = 12.1 Hz, 1 H), 3.75 and 3.70 (rotameric dd, J = 10.8, 12.1 Hz, 1 H), 3.15 and 3.01 (rotameric s, 3 H), 1.61 and 1.60 (d, J = 8.5 Hz, 1 H), 1.47−1.32 (m, 1 H), 1.24 and 1.15 (rotameric s, 3 H), 1.13 and 1.11 (rotameric s, 3 H); ^{13}C NMR (rotamers) δ 172.0, 171.8, 157.1, 157.0, 149.9, 149.1, 137.0, 136.8, 122.6, 122.3, 122.0, 120.6, 59.4, 59.3, 55.5, 52.7, 36.0, 34.0, 31.9, 31.7, 30.9, 30.4, 27.9, 27.8, 23.5, 23.1, 16.0, 15.9; IR ($CDCl_3$) ν 3406, 2950, 1622, 1476, 1435, 1405 cm^{-1}; mass spectrum (CI) m/z 249.1603 ($C_{14}H_{20}N_2O_2$ + H requires 249.1605) 231, 217, 123 (base).

[1*R*,2*S*]-1-[4-(2′-(*N*-Methyl)aminomethylpyridine)carbonyl]-3,3-dimethylcyclopropane-2-carboxaldehyde. To suspension of Dess−Martin periodinane (157 mgs, 0.37 mmol) in dry CH_2Cl_2 (2 mL) containing a catalytic amount of *tert*-butyl alcohol (2 drops) was added the alcohol **26** (73 mg, 0.29 mmol) in dry CH_2Cl_2 (1 mL). The mixture was stirred for 2 h whereupon saturated $NaHCO_3$ (1 mL) and saturated $K_2S_2O_3$ were added. The layers were separated, and the aqueous phase was extracted with CH_2Cl_2 (3 × 2 mL). The combined organics were dried ($MgSO_4$) and concentrated in vacuo, and the residue was purified via flash chromatography eluting with MeOH/CH_2Cl_2 (1:19) to give 57 mg (80%) of the *cis*-aldehyde as a pale yellow oil: ^{1}H NMR δ 9.73 and 9.67 (rotameric d, J = 6.4 Hz, 1 H), 8.61 and 8.53 (rotameric d, J = 4.4 Hz, 1 H), 7.79−7.62 (m, 1 H), 7.29−7.18 (comp, 2 H), 4.87−4.28 (m, 2 H), 3.16 and 3.06 (rotameric s, 3 H), 2.32 (rotameric d, J = 8.7 Hz, 1 H), 1.84−1.72 (m, 1 H), 1.47−1.17 (m, 6 H); ^{13}C NMR (rotamers) δ 200.62, 200.5, 169.0, 168.3, 156.7, 156.1, 149.6, 148.8, 137.0, 136.7, 122.6, 122.2, 121.9, 120.5, 55.6, 52.8, 52.4, 39.6, 39.5, 39.4, 39.1, 36.1, 34.5, 28.5, 28.3, 27.2, 27.1, 15.8, 15.6, 15.1; IR ($CDCl_3$) ν 2958, 1693, 1640, 1435 cm^{-1}; mass spectrum (CI) m/z 247.1447 ($C_{14}H_{19}N_2O_2$ + H requires 247.1446), 149, 123.

[1*R*,2*R*]-1-[4-(2′-(*N*-Methyl)aminomethylpyridine)carbonyl])-3,3-dimethylcyclopropane-2-carboxaldehyde (27). A solution of $CsCO_3$ (586 mg, 1.8 mmol) in degassed MeOH (6 mL) and the *cis*-aldehyde from the previous experiment (111 mg, 0.45 mmol) was stirred overnight at room temperature. Water (4 mL) and CH_2Cl_2 (10 mL) were added, and the layers were separated. The aqueous phase was extracted with CH_2Cl_2 (3 × 5 mL), and the combined organics were dried ($MgSO_4$) and concentrated in vacuo. The crude oily product was purified by filtration through a short plug of silica gel, eluting with MeOH/CH_2Cl_2 (5:95) to afford 109 mg (98%) of **27** as an oil: ^{1}H NMR (rotamers) δ 9.78 and 9.68 (rotameric d, J = 3.0 Hz, 1 H), 8.60 and 8.53 (rotameric d, J = 4.5 Hz, 1 H), 7.73−7.62 (m, 1 H), 7.29−7.16 (comp, 2 H), 4.87−4.63 (m, 2 H), 3.15 and 3.05 (rotameric s, 3 H), 2.71−2.68 (m, 1 H), 2.61 and 2.58 (rotameric d, J = 5.4 Hz, 1 H), 1.33 and 1.22 (rotameric s, 3 H), 1.24 and 1.14 (rotameric s, 3 H); ^{13}C NMR (rotamers) δ 200.3, 198.6, 198.2,168.7, 168.2, 157.0, 156.5, 149.7, 149.0, 136.7, 122.5, 122.2, 121.8, 120.3, 55.2, 53.0, 40.2, 39.8, 35.5, 35.0, 34.6, 32.9, 32.7, 21.0, 20.7, 19.9; IR ($CDCl_3$) ν 2957, 1702, 1639, 1477, 1110 cm^{-1}; mass spectrum (CI) m/z 247.1447 ($C_{14}H_{18}N_2O_2$ requires 247.1453), 229, 148, 123.

[1*R*,2*R*]-1-[4-(2′-(*N*-Methyl)aminomethylpyridine)carbonyl]-3,3-dimethylcyclopropane-2-carboxylic acid (28). A solution of **27** (4.8 mg, 0.0195 mmol) in acetone (0.2 mL) at 0 °C was treated with 8 N Jones reagent (9 μL) and stirred overnight. The resulting blue-green suspension was washed with brine (1 mL) and extracted with EtOAc (3 × 2 mL). The combined organics were dried ($MgSO_4$) and concentrated, and the residue was purified via flash chromatography, eluting with MeOH/AcOH/CH_2Cl_2 (5:1:94) to give 2.8 mg (55%) of **28** as a colorless oil: ^{1}H NMR (rotamers) (CD_3OD) δ 8.55 and 8.47 (rotameric d, J = 4.4 Hz, 1 H), 7.88−7.76 (m, 1 H), 7.36−7.28 (comp, 2 H), 4.85−4.70 (m, 2 H), 3.18 and 3.04 (rotameric s, 3 H), 2.43 and 2.32 (rotameric d, J = 5.6 Hz, 1 H), 2.19 and 2.18 (rotameric d, J = 5.6 Hz, 1 H), 1.16 and 1.11 and 1.10 (rotameric s, 6 H); ^{13}C NMR (rotamers) (CD_3OD) δ 174.2, 174.1, 171.9, 171.6, 158.2, 158.0, 150.6, 149.9, 146.0, 139.0, 138.9, 124.2, 123.9, 123.2, 122.6, 116.4, 56.0, 53.8, 36.5, 35.8, 35.3, 33.1, 32.9, 30.4, 30.0, 29.9, 21.4, 21.0, 20.7, 20.1; IR ($CDCl_3$) ν 2930, 1703, 1640, 1406, 1260, 1112 cm^{-1}; mass spectrum (CI) m/z 263.1396 ($C_{14}H_{18}N_2O_3$ + H requires 263.1406) 245, 161, 123.

HIV-PR Inhibitor 9. *N*-Ethyl-*N*-(dimethylaminopropyl)-carbodiimide hydrochloride (EDC) (25 mg, 0.13 mmol) was added with stirring to a solution of the carboxylic acid **20a** (30 mg, 0.12 mmol), the diamino diol **22** (20 mg, 0.067 mmol), and 1-hydroxybenzotriazole (HOBT) (36 mg, 0.27 mmol) in dry DMF (1.7 mL) at −10 °C. The reaction was then stirred for 24 h at room temperature. A portion of EtOAc (2 mL) was added, and the organic mixture was washed with brine (1 mL), 10% aqueous citric acid (1 mL), 10% aqueous $NaHCO_3$ (1 mL), and brine (1 mL). After drying ($MgSO_4$), the solvents were removed in vacuo to give 36 mg (77%) of **9** as a white solid: mp 264−267 °C; ^{1}H NMR (DMSO-d_6) δ 8.56 (t, J = 6.4 Hz, 2 H), 7.81 (d, J = 9.5 Hz, 2 H), 7.31−7.08 (comp, 20 H), 4.68 (s, 2 H), 4.60 (t, J = 9.5 Hz, 2 H), 4.22 (d, J = 6.4 Hz, 4 H), 3.17 (s, 2 H), 2.80 (dd, J = 6.4, 9.5 Hz, 2 H), 2.09 (d, J = 5.5 Hz, 2 H), 2.00 (d, J = 5.5 Hz, 2 H), 1.15 (s, 6 H), 1.12 (s, 6 H); ^{13}C NMR (CD_3OD) δ 172.5, 172.0, 140.2, 131.2, 131.0, 130.5, 130.2, 129.8, 129.4, 128.9, 128.3, 127.6, 74.3, 73.2, 52.5, 44.1, 39.2, 34.6, 34.2, 28.1, 21.2, 20.3; IR ($CHCl_3$) ν 3050, 2952, 1685, 1678 cm^{-1}; mass spectrum (FAB) m/z 759.4133 ($C_{46}H_{54}N_4O_6$ + H requires 759.4121), 741.

HIV-PR Inhibitor 10. Isolated as a white solid in 91% yield from **20b** according to the procedure described for preparing **9**: mp 285−288 °C; ^{1}H NMR (DMSO-d_6) δ 8.57 (t, J = 6.1 Hz, 2 H), 7.78 (d, J = 9.2 Hz, 2 H), 7.32−7.09 (comp, 20 H), 4.58 (s, 2 H), 4.34 (dd, J = 9.2, 15.7 Hz, 2 H), 4.26 (d, J = 6.1 Hz, 4 H), 3.16 (s, 2 H), 2.71−2.61 (m, 4 H), 1.28 (dt, J = 6.0, 9.3 Hz), 1.96−1.91 (comp, 4 H), 1.07 (d, J = 6.0 Hz, 6 H); ^{13}C NMR (CD_3OD) δ 178.1, 173.2, 137.5, 136.2, 129.9, 128.4, 128.1, 127.9, 127.7, 127.5, 127.3, 126.9, 77.2, 73.2, 52.1, 43.2, 28.2, 26.3, 23.5, 12.6, 10.2; IR ($CHCl_3$) ν 3050, 2929, 1729, 1602 cm^{-1}; mass spectrum (CI) m/z 730.3818 ($C_{44}H_{50}N_4O_6$ + H requires 731.3808), 613, 460, 307, 289, 248.

HIV-PR Inhibitor 13. To a solution of the acid **28** (26 mg, 0.099 mmol), HOBT (27 mg, 0.198 mmol), and diamino diol **22** (16.4 mg, 0.055 mmol) in DMF (1.4 mL) at −10 °C was added EDC (21 mg, 0.11 mmol), and the solution was stirred at room temperature for 24 h. EtOAc (2.8 mL) was added, and the mixture was washed with saturated $NaHCO_3$ (1 mL), water (1 mL), and brine (1 mL). The organic layer was separated, dried (Na_2SO_4), and concentrated in vacuo, and the residue was purified via flash chromatography eluting with MeOH/$CHCl_3$ (10:90) to give 26 mg (60%) of product as a white solid (mp 108−110 °C); ^{1}H NMR (CD_3OD) (rotamers) δ 8.57 & 4.47 (rotameric d, J = 5.0 Hz, 2 H), 7.90−7.76 (m, 2 H), 7.37−7.06 (comp, 14 H), 4.79−4.67 (m, 6 H), 3.12 and 3.00 (rotameric s, 6 H), 2.90−2.70 (comp, 4 H), 2.30−2.25 (m, 2 H), 2.16−2.09 (m, 2 H), 1.71−0.83 (rotameric s, 12 H); ^{13}C NMR (CD_3OD) δ 173.0, 158.3, 150.6, 139.0, 138.9, 130.4, 129.2, 127.1, 123.9, 123.0, 122.7, 74.9, 53.5, 53.1, 39.8, 36.6, 35.2, 33.5, 29.2, 29.0, 21.3, 20.9, 20.6; IR ($CHCl_3$) ν 3417, 2949, 1626, 1434, 1114 cm^{-1}; mass spectrum (CI) m/z 789.4340 ($C_{46}H_{56}N_6O_6$ + H requires 789.4328) 262, 245, 123, 120.

Kinetic Measurements of 9−13 with HIV-1 Protease. Recombinant HIV-1 protease was expressed and purified as described.[1] The K_is of **9**−**13** were determined using the fluorogenic substrate Lys-Ala-Arg-Val-Tyr-Phe(NO_2)-Glu-Ala-Nle-NH_2 using the excitation and emission maxima at 277 and 306 nm, respectively.[2] Thus, the measured K_is were 0.31−

0.35 nM for of **9**, 0.16−0.21 nM for **10**, 0.47 nM for **11**, 0.17 nM for **12**, and 80 nM for **13**. Each of these pseudopeptides was found to be a fast-binding, competitive inhibitor.

NMR Spectroscopy. Acquisition and Analysis. All spectra were recorded at 300 K on a BRUKER AMX500 spectrometer using a 18 mM natural abundance sample of **9** and a 30 mM natural abundance sample of **10** dissolved in DMSO-d_6, respectively. Temperature gradients of the ^{1}H chemical shifts were investigated by a series of 1D spectra recorded between 300 and 320 K at a proton resonance frequency of 250 MHz. Intraresidual proton and carbon assignments were obtained from TOCSY and HMQC−COSY spectra.[45] Sequential assignment of the proton spin systems was achieved by heteronuclear correlations (HMBC) supplemented by information from NOESY experiments. NOESY and ROESY spectra with mixing times of 100 and 150 ms, respectively, were recorded to generate quantitative restraints for interproton distances. NOESY and ROESY peak integrals were transformed into distance restraints using the isolated two-spin approximation (ISPA).[46] ROESY integrals were transformed after correction for offset effects.[47] To elucidate distances between protons in opposite halfs of the symmetrical molecule **9** Bzl-Cp-Phe to Phe′-Cp′-Bzl′, a ω_1-^{13}C filtered ROESY spectrum with a mixing time of 150 ms was recorded.[48] The intensitities in the ω_1 ^{13}C satellites were summed, corrected for the offset and transformed into distances using the ISPA approximation.

Homonuclear *J* values were read from absorptive in-phase signals in one-dimensional (1D) ^{1}H spectra and two-dimensional (2D) ROESY spectra using Gaussian apodization for separation of the patterns. The dihedral proton coupling of H^F across the symmetry center to $H^{F'}$ is a weak-regime coupling, when one H^F is attached to a ^{13}C nucleus in the natural abundance sample. To determine this dihedral coupling and the other proton couplings at the ^{13}C bound H^F in **9** and **10**, a 2D HMQC−COSY spectrum was recorded without ^{13}C decoupling during the acquisition (8K real points). Using the method of Kim and Prestegard,[49] approximate *J* values for the proton couplings were obtained from the proton antiphase peaks observed in the row extracted at the carbon chemical shift of C^F. The proton chemical shift of the antiphase peaks pointed to the coupling partner. Specifically, the antiphase peak in the center of the H^F ^{13}C satellites yielded an approximate value for the dihedral coupling $H^F-H^{F'}$. These approximate *J* values were readily assigned to corresponding correct *J* values determined via evaluation of the absorptive inphase pattern at one H^F ^{13}C satellite at the carbon chemical shift of C^F in a 2D HMQC spectrum, recorded without decoupling during the acquisition (8K real points).

Pairs of HMBC (mixing time 70 ms) and ^{1}H 1D spectra were analyzed for heteronuclear $^3J(^{13}C,^1H)$ coupling constants employing the peak fitting procedure of Keeler.[50] For some signals, the signal-to-noise (S/N) of ^3J-correlated peaks in the HMBC was too weak for the Keeler fitting procedure. In these cases, the value for the ^3J coupling was obtained by numerical simulation of the peak intensity in the HMBC. Input to this numerical simulation were all (^{1}H,^{1}H) couplings of the proton and one $^2J(^{13}C,^1H)$ coupling of the proton along with the integral of the $^2J(^{13}C,^1H)$ HMBC peak. Details of the simulation protocol are given in the Supporting Information. To determine the small $^3J(^{15}N,^1H)$ couplings of the cyclopropane ring protons to the nitrogens in the adjoining amide plane in **9**, a ω_1-^{15}N filtered ^{1}H−^{1}H ROESY[24] with a mixing time of 300 ms was recorded. The measuring time was 4 days to ensure a S/N of the important peaks better than 3. *J* values were read from the resulting E.COSY patterns.

Structure Calculations. The structure calculations for **9** and **10** were performed on Silicon Graphics Crimson R4000 and Indy R4600 computers. The MD calculations were carried out with the program DISCOVER 95.0 (Biosym) using the CVFF force field.[51] For the parameters of the cyclopropane ring, new atom types were defined, C^p and H^p. The geometric parameters (angles, bond lengths, and torsions) were taken from the X-ray structures of *cis*- and *trans*-3,3-dimethylcyclopropane-1,2-dicarboxylic acid[52] and from ab initio calculations of substituted cyclopropanes;[53] see Supporting Information for the detailed parameter set.

The NOE-derived distances of the symmetric molecules **9** and **10** were included as symmetry-restraints using the calculation strategy suggested by Nilges.[28] In this approach an "effective distance" is defined, which takes into account that every observed NOE cross peak in a symmetric dimer has contributions from *intra* symmetry and *inter* symmetry cross relaxation. The total NOE distance $\bar{R}_{ij}$ is described in eq 1. In our case instead of a dimer a single symmetric small molecule was analyzed. The observed signals carry contributions from distances within each half (intra) and between both halves (inter) (Figure 2).

$$\bar{R}_{ij} = \{R_{ij}^{\text{intra}-6} + R_{ij}^{\text{inter}-6}\}^{-1/6} \quad (1)$$

$\bar{R}_{ij}$: effective distance between atoms *i* and *j*

R_{ij}^{intra}: intra symmetry distance between atoms *i* and *j*

R_{ij}^{inter}: inter symmetry distance between atoms *i* and *j*

A harmonic flat bottomed potential is used for E_{noe} as given in eq 2 and is included as additional potential term to the DISCOVER 95.0 program.

$$E_{\text{NOE}} = \begin{cases} k_{ij}(r_{\text{lower}} - \bar{R}_{ij})^2 & R_{ij} < r_{\text{lower}} \\ 0 & r_{\text{lower}} \le \bar{R}_{ij} \le r_{\text{upper}} \\ k_{ij}(\bar{R}_{ij} - r_{\text{upper}})^2 & r_{\text{upper}} < \bar{R}_{ij} \end{cases} \quad (2)$$

Because of ambiguities of the NOE assignment, distance geometry calculations for the generation of an unbiased starting structure could not be performed. Therefore a three-step simulated annealing protocol was applied. In the first step the coordinates were randomized and then minimized with nonbonded terms set to zero. The second step consisted of molecular dynamics at 1000 K for 2 ps and cooling to 300 K in seven steps with the nonbonded term scaled up to normal values successively. In the third step, molecular dynamics calculations were performed for additional 2 ps at 300 K with the nonbonded term set to normal, and the resulting structure was minimized. Chiral restraints, to maintain the correct chirality, *symmetry distance restraints* as described above, and restraints form coupling constants[26,27] according to the Karplus equations[54] were included during the entire calculation. Since these initial calculations are performed in vacuo, a dielectric constant of 48.0 was applied. A total of 100 structures for each compound **9** and **10** were generated. In the case of convergence, a MD calculation in explicit solvent was performed for further refinement.

The lowest energy structure resulting from simulated annealing, was placed in a cubic box with 33 Å sides and soaked with DMSO.[55] A time step of 1 fs was maintained during all MD simulations. The minimization was separated into two steps for conjugate gradient energy minimization. In the first step the solute was fixed, and in the second step all atoms were allowed to move freely. The system was heated gradually from 50 to 300 K in 2 ps steps, each by direct velocity scaling. The system was equilibrated at 300 K for 10 ps with temperature coupling (300 K), and then configurations were saved every 100 fs for another 100 ps. During this simulation, the symmetric-distance restraints were applied with a force constant of 1 kcal Å^{-2} mol^{-1}. Additionally a harmonic ^3J coupling potential according to the Karplus equation was included.[26,27] The geometry of the symmetry center was constrained adding the experimentally derived distance restraint between Phe H^α and Phe $H^{\alpha'}$ and applying a torsion force on the central dihedral angle $H^F-H^{F'}$ of 180° with a force constant of 50 kcal/Å^{2}mol to take account for the vicinal *J* coupling constant.

The averaged structure of the restraint MD of **9** was minimized with steepest descent. The MD simulation was-continued without restraints for another 100 ps, to examine the stability of the structure defined by restrained MD.[14] The distance violations were calculated according a $\langle r^{-3}\rangle^{-1/3}$ averaging. For the distance r an *effective distance* (formula 1) was used to take account for symmetry effects.

X-ray Crystallography. Crystallization. Crystals of HIV-1 protease/10 complex were grown by vapor diffusion in hanging drops. HIV-1 protease, at 5 mg/mL in 50 mM sodium acetate buffer, pH 5.6, containing 10 mM dithiothreitol, was mixed with a stock solution of **10** in 25% DMSO to give a 1:5 molar ratio of enzyme:inhibitor at a final DMSO concentration of 5%. The crystallization well buffer consisted of 75 mM sodium citrate−150 mM sodium phosphate, pH 5.6−6.5, with 20−30% saturated ammonium sulfate. Drops were prepared by mixing equal volumes of sample and well solution, with subsequent addition of 10 μL of β-mercaptoethanol, 100 μL of DMSO, and 40 μL of 2-propanol to the well before sealing. Drops were sometimes seeded with microcrystals prior to sealing. Small crystals were used to seed hanging drops using a different well mix, 0.3 M ammonium phosphate, pH 6.2, containing 20−30% saturated ammonim sulfate, with 2−5% ethanol used as well additive prior to sealing. Crystals of suitable size for diffraction data collection grew over a period of several weeks at room temperature.

Structure Determination and Refinement. Crystals belong to the space group $P6_1$ with unit cell parameters $a = b = 63.3$ Å and $c = 83.5$ Å. X-ray diffraction data were collected from a single crystal using a MAR imaging plate area detector system and an RU-200 rotating anode X-ray generator operating at 50 kV and 100 mA. Data were processed using the program DENZO. The data are 49% complete to 2.0 Å and 70% complete to 2.5 Å with a merging R factor of 5.6% overall. A total of 6154 unique reflections with $|F|/\sigma > 2.0$ in the resolution range 7−2.0 Å were used in the structure determination and refinement. The crystal structure was solved by molecular replacement using the protein coordinates of HIV-PR complexed with PD99560[57] and refined to a final R factor of 18.5% using the program X-PLOR 3.1. The inhibitor was initially built using QUANTA (Molecular Simulations, Inc. Cambridge, MA) and fitted to the difference electron density map calculated using the phases from the refined protein structure. Refinement statistics are listed in Table 1.

Model Calculations for the Cyclopropane Diols. Ab initio calculations were performed using Hartree−Fock (HF) and density functional theory (DFT) methods with the 6-31G* basis set as implemented in the Gaussian 94 program package.[32] For all DFT calculations, hybrid B3LYP exchange correlation potentials were included with the 6-31G* basis set.[33,34] Optimizations at the semiempirical level used AM1 and PM3 methods as implemented in the MNDO94 program suite in UniChem 3.0. Solvation free energies were calculated using a reaction field approach based on the boundary element method (BEM).[58] The effective atomic charges used for the BEM calculations of solvation energies were obtained from fitting the electrostatic potentials, calculated using DFT at the B3LYP/6-31G* level, for each optimized structure in its gas-phase geometry.

Acknowledgment. We are grateful for generous financial support from the National Institutes of Health, the Robert A. Welch Foundation, the Texas Advanced Technology Program, Alexander von Humboldt Foundation (S.F.M.), the Deutsche Forschungsgemeinschaft and the Fonds der chemischen Industrie (H.K.), and the National Cancer Institute (J.W.E.). We also thank Drs. Dale J. Kempf and Norman E. Wideburg (Abbott Laboratories) for preliminary biological testing of compounds **9** and **10**. The content of this publication does not necessarily reflect the view or policies of the Department of Health and Human Services, nor does mention of tradenames, commercial products, or organization imply endorsement by the U. S. Government.

Supporting Information Available: Experimental procedures and spectral data for compounds **11** and **12** and intermediates in their synthesis, detailed NMR assignments for **9** and **10**, parameters for the cyclopropane used in the MD calculations, and descriptions of techniques used to handle ambiguous NOE data and to determine hetero coupling constants from the HMBC spectrum (11 pages). Ordering information is given on any current masthead page.

References

(1) Notable cases are found in the structures of immunosupressants and their complexes. Cyclosporin A. Solution and X-ray: (a) Loosli, H. R.; Kessler, H.; Oschkinat, H.; Petcher, H. P.; Weber, T. J.; Widmer A. 76. Peptide Conformations. The Conformation of Cyclosporin A in the Crystal and in Solution. *Helv. Chim. Acta* **1985**, *68*, 682−704. (b) Kessler, H.; Köck, M.; Wein, T.; Gehrke, M. 164. Reinvestigation of the Conformatin of Cyclosporin A in Chloroform. *Helv. Chim. Acta* **1990**, *73*, 1818−1832. Complex: (c) Weber, C.; Wider, G.; von Freyberg, B.; Traber, R.; Braun, W.; Widmer, H.; Wüthrich, K. The NMR Structure of Cyclosporin A Bound to Cyclophilin in Aqueous Solution. *Biochemistry* **1991**, *30*, 6563−6574. (d) Fesik, S. W.; Gampe, R. T.; Eaton, H. L.; Gemmecker, G.; Olejniczak, E. T.; Neri, P.; Holzman, T. F.; Egan, D. A.; Edalji, R.; Simmer, R.; Helfrich, R.; Hochloewski, J.; Jackson, M. NMR Studies of [U-^{13}C]Cyclosporin A Bound to Cyclophilin: Bound Conformation and Portions of Cyclosporin Involved in Binding. *Biochemistry* **1991**, *30*, 6574−6583. FK506. Solution and X-ray: (e) Karuso, P.; Kessler, H.; Mierke, D. F. Solution Structure of FK506 from Nuclear Magnetic Resonance and Molecular Dynamics. *J. Am. Chem. Soc.* **1990**, *112*, 9434−9436. (f) Siekerka, J. J.; Hung, S. H. Y.; Poe, M.; Lin, C. S.; Sigal, N. H. A Cytosolic Binding Protein for the Immunosuppressant FK506 has Peptidyl-Prolyl Isomerase Activity but is Distinct from Cyclophilin. *Nature* **1989**, *341*, 755−757. Complex: (g) van Duyne, G. D.; Standaert, R. F.; Karplus, P. A.; Schreiber, S. L.; Clardy, J. Atomic Structure of FKBP−FK506, an Immunophilin Immunosuppressant Complex. *Science* **1991**, *252*, 839−842.

(2) (a) Kessler, H. NMR-spektroskopishe Methoden Zur Konformationanayse von Peptiden. (Conformations and Biological Activity of Cyclic Peptides.) *Angew. Chem., Int. Ed. Engl.* **1982**, *21*, 512−523. (b) Hruby, V. J. Conformational Restrictions of Biologically Active Peptides via Amino Acid Side Chain Groups. *Life Sci.* **1982**, *31*, 189−199. (c) Toniolo, C. Conformationally Restricted Peptides Through Short-Range Cyclizations. *Int. J. Pept. Protein Res.* **1990**, *35*, 287−300.

(3) (a) Spatola, A. F. Peptide Backbone Modifications: A Structure−Activity Analysis of Peptides Containing Amide Bond Surrogates. Conformational Constraints, and Related Backbone Replacements. In *Chemistry and Biochemistry of Amino Acids, Peptides, and Proteins;* Weinstein, B., Ed.; Marcel Dekker, New York, 1983; Vol. 7, pp 267−357. (b) Hruby, B. J.; Al-Obeidi, F.; Kazmierski, W., Emerging Approaches in the Molecular Design of Receptor-Selective Peptide Ligands: Conformational, Topographical and Dynamic Considerations. *Biochem. J.* **1990**, *268*, 249−262. (c) Olson, G. L.; Bolin, D. R.; Bonner, M. P.; Bös, M.; Cook, C. M.; Fry, D. C.; Graves, B. J.; Hatada, M.; Hill, D. E.; Kahn, M.; Madison, V. S.; Ruisiecki, V. K.; Sarabu, R.; Sepinwall, J.; Vincent, G. P.; Voss, M. E. Concepts and Progress in the Development of Peptides Mimics. *J. Med. Chem.* **1993**, *36*, 3039−3049. (d) Giannis, A.; Kolter, T. Peptidomimetics for Receptor Ligands. Discovery, Development, and Medical Perspectives. *Angew. Chem., Int. Ed. Eng.* **1993**, *32*, 1244−1267. (e) Gante, J. Peptidomimetics-Tailored Enzyme Inhibitors. *Angew. Chem., Int. Ed. Eng.* **1994**, *33*, 1699−1720. (f) Wiley, R. A.; Rich, D. H. Peptidomimetics Derived from Natural-Products. *Med. Res. Rev.* **1993**, *13*, 327−384. (g) Adang, A. E. P.; Hermkens, P. H. H.; Linders, J. T. M.; Ottenheijm, H. C. J.; van Staveren, C. J. Case Histories of Peptidomimetics. Progression from Peptides to Drugs. *Recl. Trav. Chim. Pays-Bas* **1994**, *113*, 63−78.

(4) (a) Ball, J. B.; Alewood, P. F. Conformational Constraints: Nonpeptide β-Turn Mimics. *J. Mol. Recognit.* **1990**, *3*, 55−64. (b) Kahn, M. Peptide Secondary Structure Mimetics: Recent Advances and Future Challenges. *SynLett.* **1993**, 821−826.

(5) Mueller, K.; Obrecht, D.; Knierzinger, A.; Stankovic, C.; Spiegler, C.; Bannwarth, W.; Trzeciak, A; Englert, G.; Labhardt, A. M.; Schönholzer, P. Building Blocks for the Induction or Fixation of Peptide Conformations. In *Perspectives in Medicinal Chemistry*; Testa, B., Fuhrer, W., Kyburz, E., Giger, R., Eds.; VCH: Weinheim, Germany, 1993; pp 513−532.

(6) For example, see: (a) Hagihara, M.; Anthony, N. J.; Stout, T. J.; Clardy, J.; Schreiber, S. L. Vinylogous Polypeptides: An Alternative Peptide Backbone. *J. Am. Chem. Soc.* **1992**, *114*, 6568−6570. (b) Smith, A. B., III; Keenan, T. P.; Holcomb, R. C.;

Sprengeler, P. A.; Guzman, M. C.; Wood, J. L.; Carroll, P. J.; Hirschmann, R. Design, Synthesis, and Crystal Structure of a Pyrrolinone-Based Peptidomimetic Possessing the Conformation of a β-Strand: Potential Application to the Design of Novel Inhibitors of Proteolytic Enzymes, *J. Am. Chem. Soc.* **1992**, *114*, 10672−10674. (c) Chen, L.; Trilles, R. V. Asymmetric Synthesis of a Novel Phenylogous Amino Acid Mimicking an Extended Dipeptide. *Tetrahedron Lett.* **1992**, *36*, 8715−8718. (d) Boumendjel, A.; Roberts, J. C.; Hu, E.; Pallai, P. V.; Rebek, J., Jr. Design and Asymmetric Synthesis of β-Strand Peptidomimetics. *J. Org. Chem.* **1996**, *61*, 4434−4438. (e) Janetka, J. W.; Raman, P.; Satyshur, K.; Flentke, G. R.; Rich, D. H. Novel Cyclic Biphenyl Ether Peptide β-Strand Mimetics and HIV-Protease Inhibitors. *J. Am. Chem. Soc.* **1997**, *119*, 441−442.

(7) For the fixation of the side chain orientation of Phe see (a) Zechel, C.; Kessler, H.; Geiger, R. Synthesis and Conformational Studies of Enkephalin-like Cyclic Peptides and Depsipeptides. In *Peptides, Structure and Function (Proceedings of the 9th American Peptide Symposium)*; Deber, C. M., Hruby, V. J., Kopple, K. D., Eds.; Pierce Chemical Co.: Rockford, IL, 1985; pp 507−510. (b) Tourwe, D.; Verschueren, K.; Frycia, A.; Davis, P.; Porreca, F.; Hruby, V. J.; Toth, G.; Jaspers, H.; Verheyden, P.; van Binst, G. Conformational Restriction of Tyr and Phe Side Chains in Opioid Peptides: Information About Preferred and Bioactive Side-Chain Topology. *Biopolymers* **1996**, *38*, 1−12.

(8) For reviews, see: (a) Stammer, C. H. Cyclopropane Amino Acids (2,3- and 3,4-Methanoamino Acids). *Tetrahedron* **1990**, *46*, 2231−2254. (b) Burgess, K.; Ho,, K.-K.; Moye-Sherman, D. Asymmetric Syntheses of 2,3-Methanoamino Acids. *SynLett.* **1994**, 575−583.

(9) See also: Melnick, M. J.; Bisaha, S. N.; Gammill, R. B., Conformationally Restricted $P_1-P_{1'}$ Transition State Analogues. Synthesis of 1(*R*), 3(*R*) [1(*S*), 2(*S*)] 3-[3-Cyclohexyl-2-[(Boc)-amino]-1-hydroxypropyl]-2,2-dimethylcyclopropane Carboxylic Acids. *Tetrahedron Lett.* **1990**, *31*, 961−964.

(10) (a) Chesnut, D. B.; Marsh, R. E. The Crystal Structure of Cyclopropanecarbohydrazide. *Acta Crystallogr.* **1958**, *11*, 413−419. (b) Long, R. E.; Maddox, H.; Trueblood, K. N. The Crystal and Molecular Structure of Cyclopropanecarboxamide. *Acta Crystallogr.* **1969**, B*25*, 2083−2094. (c) Lynch, V. M.; Austin, R. E.; Martin, S. F.; George, T. Determination of the Absolute Configuration of a Novel Dipeptide Isostere. *Acta Crystallogr.* **1991**, C*47*, 1345−1347. (d) Itai, A.; Toriumi, Y.; Saito, S.; Kagechika, H.; Shudo, K. Preference of *cis*-Amide Structure in *N*-Acyl-*N*-methylanilines. *J. Am. Chem. Soc.* **1992**, *114*, 10649−100650.

(11) (a) Page, M. I.; Jencks, W. P. Entropic Contributioins to Rate Accelerations in Enzymatic and Intramolecular Reactions and the Chelate Effect. *Proc. Natl. Acad. Sci. U.S.A.* **1971**, *68*, 1678−1683. (b) Jencks, W. P. On the Attribution and Additivity of Binding Energies. *Proc. Natl. Acad. Sci. U.S.A.* **1981**, *78*, 4046−4050. (c) Searle, M. S.; Williams, D. H. The Cost of Conformational Order: Entropy Changes in Molecular Associations. *J. Am. Chem. Soc.* **1992**, *114*, 10690−10697. (d) Gerhard, U.; Searle, M. S.; Williams, D. H. The Free Energy Change of Restricting a Bond Rotation in the Binding of Peptide Analogues to Vancomycin Group Antibiotics. *BioMed. Chem. Lett.* **1993**, *3*, 803−808 and references therein.

(12) (a) Fersht, A. R., The Hydrogen Bond in Molecular Recognition. *Trends Biol. Sci.* **1987**, *12*, 301−304. (b) Searle, M. S.; Williams, D. H.; Gerhard, U. Partitioning of Free Energy Contributions in the Estimation of Binding Constants: Residual Motions and Consequences for Amide-Amide Hydrogen Bond Strengths. *J. Am. Chem. Soc.* **1992**, *114*, 10697−10704. (c) Kato, Y.; Conn, M. M.; Rebek, Jr., J. Hydrogen Bonding in Water Using Synthetic Receptors. *Proc. Natl. Acad. Sci. U.S.A.* **1995**, *92*, 1208−1212.

(13) (a) Martin, S. F.; Austin, R. E.; Oalmann, C. J.; Baker, W. R.; Condon, S. L.; DeLara, E.; Rosenberg, S. H.; Spina, K. P.; Stein, H. H.; Cohen, J.; Kleinert, H. D. 1,2,3-Trisubstituted Cyclopropanes as Conformationally Restricted Peptide Isosteres: Application to the Design and Synthesis of Novel Renin Inhibitors. *J. Med. Chem.* **1992**, *35*, 1710−1721. (b) Baker, W. R.; Jae, H.-S.; Martin, S. F.; Condon, S. L.; Stein, H. H.; Cohen, J.; Kleinert, H. D. Conformationally Restricted Peptide Isosteres. 2. Synthesis and In Vitro Potency of Dipeptide Renin Inhibitors Employing a 2-Alkylsulfonyl-3-Phenylcyclopropane Carboxamide as a P_3 Amino Acid Replacement. *Bioorg. Med. Chem. Lett.* **1992**, *2*, 1405.

(14) Martin, S. F.; Oalmann, C. J.; Liras, S. Cyclopropanes as Conformationally Restricted Peptide Isosteres. Design and Synthesis of Novel Collagenase Inhibitors, *Tetrahedron* **1993**, *49*, 3521−3532.

(15) Bovy, P. R.; Tjoeng, F. S.; Rico, J. G.; Rogers, T. E.; Lindmark, R. J.; Zablocki, J. A.; Garland, R. B.; McMackins, D. E.; Dayringer, H.; Toth, M. V.; Zupec, M. E.; Rao, S.; Panzer-Knodle, S. G.; Nicholson, N. S.; Salyers, A.; Taite, B. B.; Herin, M.; Miyano, M.; Feigen, L. P.; Adams, S. P. Design of Orally, Active, Non-Peptide Fibrinogen Receptor Antagonists. An Evolutionary Process from the RGD Sequence to Novel Anti-Platelet Aggregation Agents. *Bioorg. Med. Chem.* **1994**, *2*, 881−895.

(16) For a review HIV-1 protease inhibitors, see: (a) Huff, J. R. HIV Protease: A Novel Chemotherapeutic Target for AIDS. *J. Med. Chem.* **1991**, *34*, 2305−2314. See also: (b) Dreyer, G. B.; Lambert, D. M.; Meek, T. D.; Carr, T. J.; Tomaszek, T. A., Jr.; Fernandez, A. V.; Bartus, H.; Cacciavillani, E.; Hassell, A. M.; Minnich, M.; Petteway, S. R., Jr.; Metcalf, B. W. Hydroxyethylene Isostere Inhibitors of Human Immunodeficiency Virus-1 Protease: Structure−Activity Analysis Using Enzyme Kinetics, X-ray Crystallography, and Infected T-Cell Assays. *Biochemistry* **1992**, *31*, 6646−6659. (c) Thompson, W. J.; Fitzgerald, P. M. D.; Holloway, M. K.; Emini, E. A.; Drake, P. L.; McKeever, B. M.; Schleif, W. A.; Quintero, J. C.; Zugay, J. A.; Tucker, T. J.; Schwering, J. E.; Homnick, C. F.; Nunberg, J.; Springer, J. P.; Huff, J. R. Synthesis and Antiviral Activity of a Series of HIV-1 Protease Inhibitors with Functionality Tethered to the P_1 or $P_{1'}$ Phenyl Substituents: X-ray Crystal Structure Assisted Design. *J. Med. Chem.* **1992**, *35*, 1685−1701. (d) Kempf, D. J.; Codacovi, L.; Wang, X. C.; Kohlbrenner, W. E.; Wideburg, N. E.; Saldivar, A.; Vasavanonda, S.; March, K. C.; Bryant, P.; Sham, H. L.; Green, B. E.; Betebenner, D. A.; Erickson, J.; Norbeck, D. W. Symmetry-Based Inhibitors of HIV Protease. Structure−activity Studies of Acylated 2,4-Diamino-1,5-diphenyl-3-hydroxypentane and 2,5-Diamino-1,6-diphenylheane-3,4-diol. *J. Med. Chem.* **1993**, *36*, 320−330. (e) Thaisrivongs, S.; Turner, S. R.; Strohbach, J. W.; TenBrink, R. E.; Tarpley, W. G.; McQuade, T. J.; Heinrikson, R. L.; Tomasselli, A. G.; Hui, J. O.; Howe, W. J. Inhibitors of the Protease from Human Immunodeficiency Virus: Synthesis, Enzyme Inhibition, and Antiviral Activity of a Series of Compounds Containing the Dihydroxyethylene Transition−State Isostere. *J. Med. Chem.* **1993**, *36*, 941−952. (f) Waller, C. L.; Oprea, T. I.; Giolitti, A.; Marshall, G. R. Three-Dimensional QSAR of Human Immunodeficiency Virus (I) Protease Inhibitors. 1. A CoMFA Study Employing Experimentally-Determined Alignment Rules. *J. Med. Chem.* **1993**, *36*, 4152−4160. (g) Lam, P. Y. S.; Jadhav, P. K.; Eyermann, C. J.; Hodge, C. N.; Ru, Y.; Bacheler, L. T.; Meek, J. L.; Otto, M. J.; Rayner, M. M.; Wong, Y. N.; Chang, C.-H.; Weber, P. C.; Jackson, D. A.; Sharpe, T. R.; Erickson−Viitanen, S. Rational Design of Potent, Bioavailable, Nonpeptide Cyclic Ureas as HIV Protease Inhibitors. *Science* **1994**, *263*, 380−384. (h) Smith, A. B., III; Hirschmann, R.; Pasternak, A.; Guzman, M. C.; Yokoyama, A.; Sprengeler, P. A.; Darke, P. L.; Emini, E. A.; Schleif, W. A. Pyrrolinone-Based HIV Protease Inhibitors. Design, Synthesis and Antiviral Activity: Evidence for Improved Transport. *J. Am. Chem. Soc.* **1995**, *117*, 11113−11123.

(17) Leading references to structural studies of HIV-1 protease, see: (a) Miller, M.; Swain, A. L.; Jaskólski, M.; Sathyanarayana, B. K.; Marshall, G. R.; Rich, D. H.; Kent, S. B. H.; Wlodawer, A. X-ray Analysis of HIV-1 Protease and Its Complexes with Inhibitors. In *Retroviral Proteases: Control of Maturation and Morphogenesis;* Pearl, L., Ed; Macmillan Press: New York, 1990, p 93−106. (b) Wlodawer, A., Erickson, J. W. Structure-Based Inhibitors of HIV-1 Protease. *Annu. Rev. Biochem.* **1993**, *62*, 543−585. (c) Dreyer, G. B.; Boehm, J. C.; Chenera, B.; DesJarlais, R. L.; Hassell, A. M.; Meek, T. D.; Tomaszek, T. A., Jr. A Symmetric Inhibitor Binds HIV-1 Protease Asymmetrically. *Biochemistry* **1993**, *32*, 937−947. (d) Hosur, M. V.; Bhat, T. N.; Kempf, D. J.; Baldwin, E. T.; Liu, B.; Gulnik, S.; Wideburg, N. E.; Norbeck, D. W.; Appelt, K.; Erickson, J. W. Influence of Stereochemistry on Activty and Binding Modes for C_2 Symmetry-Based Diol Inhibitors of HIV-1 Protease. *J. Am. Chem. Soc.* **1994**, *116*, 847−855. (e) Smith, A. B., III; Hirschmann, R.; Pasternak, A.; Yao, W. Sprengeler, P. A.; Holloway, M. K.; Kuo, L. C.; Chen, Z.; Darke, P. L.; Schleif, W. A. An Orally Bioavailable Pyrrolinone Inhibitor of HIV-1 Protrease: Computational Analysis and X-ray Crystal Structure of the Enzyme Complex. *J. Med. Chem.* **1997**, *40*, 2440−2444.

(18) Kempf, D. J.; Sowin, T. J.; Doherty, E. M.; Hannick, S. M.; Codavoci, L.; Henry, R. F.; Green, B. E.; Spanton, S. G.; Norbeck, D. W. Stereocontrolled Synthesis of C_2-Symmetric and Pseudo-C_2-Symmetric Diamino Alcohols and Diols for Use in HIV Protease Inhibitors. *J. Org. Chem.* **1992**, *57*, 5692−5700.

(19) (a) Doyle, M. P.; Pieters, R. J.; Martin, S. F.; Austin, R. E.; Oalmann, C. J.; Müller, P. High Enantioselectivity in the Intramolecular Cyclopropanation of Allyl Diazoacetates Using a Novel Rhodium(II) Catalyst. *J. Am. Chem. Soc.* **1991**, *113*, 1423−1424. (b) Martin, S. F.; Spaller, M. R.; Liras, S.; Hartmann, B. Enantio- and Diastereoselectivity in the Intramolecular Cyclopropanation of Secondary Allylic Diazoacetates. *J. Am. Chem. Soc.* **1994**, *116*, 4493−4494. (c) Doyle, M. P.; Austin, R. E.; Bailey, A. S.; Dwyer, M. P.; Dyatkin, A. B.; Kalinin, A. V.; Kwan, M. M. Y.; Liras, S.; Oalmann, C. J.; Pieters, R. J.; Protopopova, M. N.; Raab, C. E.; Roos, G. H. P.; Zhou, Q.-L.;

Martin, S. F. Enantioselective Intramolecular Cyclopropanations of Allylic and Homoallylic Diazoacetates and Diazoacetamides Using Chiral Dirhodium (II) Carboxamide Catalysts. *J. Am. Chem. Soc.* **1995**, *117*, 5763−5775.
(20) Corey, E. J.; Myers, A. G. Efficient Synthesis and Intramolecular Cyclopropanation of Unsaturated Diazoacetic Esters. *Tetrahedron Lett.* **1984**, *23*, 3559−3562.
(21) (a) Basha, A.; Lipton, M.; Weinreb, S. M. A Mild, General Method for Conversion of Esters to Amides. *Tetrahedron Lett.* **1977**, 4171−4174. (b) Sibi, M. P. Chemistry of *N*-Methoxy-*N*-Methylamides. Application in Synthesis. A Review. *Org. Prep. Proc. Int.* **1993**, *25*, 15−40.
(22) This mixture of **18c** and **20** could not be readily separated, but the corresponding carboxylic acids could be easily separated by flash chromatography.
(23) Schleucher, J.; Quant, J.; Glaser, S. J.; Griesinger, C. A Theorem Relating Cross Relaxation and Hartmann−Hahn Transfer in Multiple-Pulse Sequences. Optimal Suppression of TOCSY Transfer in ROESY. *J. Magn. Reson. A* **1995**, *112*, 144−151.
(24) Eberstadt, M; Gemmecker, G.; Mierke, D. F.; Kessler, H. Scalar Coupling Constants- Their Analysis and Their Application for the Elucidation of Structures. *Angew. Chem., Int. Ed. Engl.* **1995**, *34*, 1671−1695.
(25) Kim Y.; Prestegard, J. H. Motional Properties of Acyl Carrier Protein: Effects on NMR Structural Data. *Proteins Struct. Funct. Genet.* **1990**, *8*, 377−385.
(26) Mierke, D. F.; Kessler, H. Improved Molecular Dynamics Simulations for the Determination of Peptide Structures. *Biopolymers* **1993**, *33*, 1003−1017.
(27) Mierke, D. F.; Kessler, H. Combined Use of Homo- and Heteronuclear Coupling Constants as Restraints in Molecular Dynamics Simulations. *Biopolymers* **1992**, *32*, 1277−1282.
(28) Nilges, M. A Calculation Strategy for the Structure Determination of Symmetrical Dimers by ^{1}H NMR. *Proteins: Struct. Funct. Genet.* **1993**, *17*, 297−309.
(29) Wüthrich, K.; Billeter, M.; Braun, W. Sequential Resonance Assignments in Protein Proton Nuclear Magnetic Resonanace Spectra. Computation of Sterically Allowed Proton−Proton Distances and Statistical Analysis of Proton−Proton Distances in Single-Crystal Protein Conformations. *J. Mol. Biol.* **1983**, *169*, 946−961.
(30) Kessler, H.; Schmitt, W. in *Encyclopedia of Nuclear Magnetic Resonance*; Grant, D. M., Harris, R. K., Eds.; John Wiley & Sons: Chichester, England, 1996; Vol. 6, pp 3527−3537.
(31) (a) Pachler, K. G. R. Nuclear Magnetic Resonance (NMR) Study of Some α-Amino Acids. I. Coupling Constants in Alkaline and Acid Medium. *Spektochim. Acta* **1963**, *19*, 2085−2092. (b) Pachler, K. G. R. Nuclear Magnetic Resonance Study of Some α-Amino Acids. II. Rotational Isomerism. *Spektochim. Acta* **1964**, *20*, 581−587.
(32) Frisch, M. J.; et al. *Gaussian 94 (Revision D.4)*; Gaussian, Inc.: Pittsburgh, PA, 1995.
(33) Becke, A. D. Universality in the Peroxidase-Oxidase Reaction: Period Doublings, Chaos, Period Three, and Unstable Limit Cycles. *J. Phys. Chem.* **1993**, *98*, 5648−5642.
(34) Lee, C.; Yang, W.; Parr, R. G. Various Functionals for the Kinetic Energy Density of an Atom or Molecule. *Phys. Rev.* **1988**, *B37*, 785−789.
(35) Baldwin, E. T.; Bhat, T. N.; Gulnik, S. V.; Liu, B.; Topol, I. A.; Kiso, Y.; Mimoto, T.; Mitsuya, H.; Erickson, J. W. Structure of HIV-1 Protease with KN-272, a Tight Binding Allophenylnorstatine. *Structure* **1995**, *3*, 581−590.
(36) Ohno, Y.; Kiso, Y.; Kobayashi, Y. Solution Conformations of KNI-272, a Tripeptide HIV Protease Inhibitor Designed on the Basis of Substrate Transition State: Determinated by NMR Spectroscopy and Simulated Annealing Calculations. *Bioorg. Med. Chem.* **1996**, *4*, 1565−1572.
(37) Preuss, R.; Schmidt, R. R. *C*-Glucoside Durch Direkte 1-*C*-Lithiierung von 2-Phenylsulfinyl Aktiviertem *D*-Glucal. (*C*-Glycosides from Direct C(1)-Lithiation of 2-Phenylsulfinyl Activated *D*-Glucals.) *Liebigs Ann. Chem.* **1989**, 429−434.
(38) Tan, B.; Chia, L. H. L.; Huang, H.; Kuok, M.; Tang, S. Rotational Isomerism in 2,3-Dinitro-2,3-dimethylbutane. *J. Chem. Soc., Perkin Trans.* **1984**, *2*, 1407−1415.
(39) Topol, I. A., unpublished results.
(40) (a) de Meijere, A. Bonding Properties of Cyclopropane and Their Chemical Consequences. *Angew. Chem., Int. Ed. Eng.* **1979**, *18*, 809−826. (b) Jorgenson, M. J.; Leung, T. Cyclopropyl Conjugation in Olefinic Esters. Conformational Effects on Ultraviolet Absorption. *J. Am. Chem. Soc.* **1968**, *90*, 3769−3774.
(41) Hoffmann, R. W. Flexible Molecules with Defined Shape-Conformational Design. *Angew. Chem., Int. Ed. Engl.* **1992**, *31*, 1124−1134.
(42) Bhat, T. N.; Baldwin, E. T.; Liu, B.; Cheng, Y.-S. E.; Erickson, J. W. Crystal-Structure of a Tethered Dimer of HIV-1 Proteinase Complexed with an Inhibitor. *Nat. Struct. Biol.* **1994**, *1*, 552−556.
(43) Gulnik, S. V.; Suvorov, L. I.; Liu, B.; Anderson, B.; Mitsuya, H., Erickson, J. W. Kinetic Characterization and Cross-Resistance Patterns of HIV-1 Protease Mutants Selected under Drug Pressure. *Biochemistry* **1995**, *34*, 9282−9287.
(44) Kageyama, S.; Mimoto, T.; Murakawa, Y.; Nomizu, M.; Ford, H., Jr.; Shirasaka, T.; Gulnik, S.; Erickson, J.; Takada, K.; Hayashi, H.; Broder, S.; Kiso, Y.; Mitsuya, H. Invitro Anti-Human-Immunodeficiency-Virus (HIV) Activities of Transition-State HIV Protease Inhibitors Containing Allophenylnorstatine. *Antimicrob. Agents Chemother.* **1993**, *37*, 810−817.
(45) Kessler, H.; Gehrke, M.; Griesinger, C. Two-Dimensional NMR Spectroscopy: Background and Overview of the Experiments. *Angew. Chem., Int. Ed. Engl.* **1988**, *27*, 490−536.
(46) Neuhaus, D.; Williamson, M. *The Nuclear Overhauser Effect in Structural and Conformational Analysis*; VCH: Weinheim, Germany, 1989.
(47) Griesinger, C.; Ernst, R. R. Frequency Offset Effects and Their Elimination in NMR Rotating-Frame Cross-Relaxation Spectroscopy. *J. Magn. Reson.* **1987**, *75*, 261−271.
(48) Otting, G.; Wüthrich, K. Heteronuclear Filters in Two-Dimensional [Proton-Proton]-NMR Spectroscopy: Combined Use with Isotope Labelling for Studies of Macromolecular Conformation and Intermolecular Interactions. *Q. Rev. Biophys.* **1990**, *23*, 39−96.
(49) Kim, Y.; Prestegard, J. H. Measurement of Vicinal Couplings from Cross Peaks in COSY Spectra. *J. Magn. Reson.* **1989**, *84*, 9−13.
(50) Keeler, J.; Neuhaus, D.; Titman J. J. A Convenient Technique for the Measurement and Assignment of Long-Range Carbon-13 Proton Coupling Constants. *J. Chem. Phys.* **1988**, *146*, 545−548.
(51) (a) Hagler, A. T.; Lifson, S.; Dauber, P. Consistent Force Field Studies on Intramolecular Forces in Hydrogen-Bonded Crystals. 2. A Benchmark for the Objective Comparison of Alternative Force Fields. *J. Am. Chem. Soc.* **1979**, *101*, 5122−5130. (b) DISCOVER Version 95.0, Biosym Technologies, 10065 Barnes Canyon Road, San Diego, CA 92121, USA.
(52) Jessen, S. M. Structure of Two Cyclopropane Derivatives: cis- and *trans*-Caronic Acid. *Acta Crystallogr., C* **1992**, *48*, 106−116.
(53) (a) Cremer, D.; Gauss, J. Theoretical Determination of Molecular Structure and Conformation. 20. Reevaluation of the Strain Energies of Cyclopropane and Cyclobutane-CC and CH Bond Energies, 1,3 Interactions, and σ-Aromticity. *J. Am. Chem. Soc.* **1986**, *108*, 7467−7477. (b) Cremer, D.; Gauss, J. Theoretical Determination of Molecular Structure and Conformation. 16. Substituted Cyclopropanes-An Electron Density Model of Substituent-Ring Interactions. *J. Am. Chem. Soc.* **1985**, *107*, 3811−3819.
(54) (a) Bystrov, V. F. Spin−Spin Coupling and the Conformational States of Peptide Systems. *Prog. Nucl. Magn. Reson. Spectrosc.* **1976**, *10*, 41−81. (b) Kessler, H.; Griesinger, C.; Wagner, K. Peptide Conformations. 42. Conformation of Side Chains in Peptides Using Heteronuclear Coupling Constants Obtained by Two-Dimensional NMR Spectroscopy. *J. Am. Chem. Soc.* **1987**, *109*, 6927−6933. (c) Wang, A. C.; Bax, A. Reparametrization of the Karplus Relation for $^3J(H^{\alpha}-N)$ and $3J(H^N-C^1)$ in Peptides Form Uniformly $^{13}C/^{15}N$-Enriched Human Ubiquitin. *J. Am. Chem. Soc.* **1995**, *117*, 1810−1813. (d) Wang, A. C.; Bax, A. Determination of the Backbone Dihedral Angles ϕ in Human Ubiquitin from Reparameterixed Emperical Karplus Equations. *J. Am. Chem. Soc.* **1996**, *118*, 2483−2494.
(55) Mierke, D. F.; Kessler, H. Molecular Dynamics with Dimethyl Sulfoxide as a Solvent. Conformation of a Cyclic Hexapeptide. *J. Am. Chem. Soc.* **1991**, *113*, 9466−9470.
(56) Saulitis, J.; Mierke, D. F.; Byk, G.; Gilon, C.; Kessler, H. Conformation of Cyclic Analogues of Substance P: NMR and Molecular Dynamics in Dimethyl Sulfoxide. *J. Am. Chem. Soc.* **1992**, *114*, 4818−4827.
(57) Lunney, E. A.; Hagen, S. E. Domagala, J. M.; Humblet, C.; Kosinski, J.; Tait, B. D.; Warmus, J. S.; Wilson, M.; Ferguson, D.; Hupe, D.; Tummino, P. J.; Baldwin, E. T.; Bhat, T. N.; Liu, B.; Erickson, J. W. A Novel Nonpeptide HIV-1 Protease Inhibitor: Elucidation of the Binding Mode and Its Application in the Design of Related Analogs. *J. Med. Chem.* **1994**, *37*, 2664−2677.
(58) Rashin, A. A. Aspects of Protein Energetics and Dynamics. *Prog. Biophys. Mol. Biol.* **1993**, *70*, 73−200.

JM980033D